



Poly(L-lactide-co- ϵ -caprolactone)/gelatin-based small-diameter vascular grafts: Salutatory effect of the BVLD and EGCG-Cu to promote hemocompatibility and nitric oxide production for *in situ* blood vessel regeneration

Guangfang Cai^{a,1}, Zhengchao Yuan^{a,1}, Xinyi Wang^{a,1}, Siyuan Wu^b, Shasha Zhou^a, Zheng Lei^a, Peng Li^b, Mohamed EL-Newehy^d, Meera Moydeen Abdulhameed^d, Muhammad Shafiq^{c,*}, Xiumei Mo^{a,*}, Shichao Jiang^{b,*}, Hongbing Gu^{e,*}

^a State Key Laboratory for Modification of Chemical Fibers and Polymer Materials, Shanghai Engineering Research Center of Nano-Biomaterials and Regenerative Medicine, College of Chemistry, Chemical Engineering and Biotechnology, Donghua University, Shanghai 201620, PR China

^b Department of Orthopedics, Shandong Provincial Hospital Affiliated to Shandong First Medical University, Jinan 250021, PR China

^c Innovation Center of NanoMedicine (iCONM), Kawasaki Institute of Industrial Promotion, Kawasaki-ku, Kawasaki 210-0821, Japan

^d Department of Chemistry, College of Science, King Saud University, P.O. Box 2455, Riyadh 11451, Saudi Arabia

^e Department of Cardiovascular Surgery, Shanghai General Hospital, Shanghai Jiaotong University School of Medicine, No. 650 Xinsongjiang Rd., Shanghai 201600, PR China

ARTICLE INFO

Keywords:

SDVGs
EGCG-Cu
BVLD
Anti-thrombosis
Electrospinning

ABSTRACT

Polymeric small-diameter vascular grafts (SDVGs, inner diameter, < 6 mm) with characteristics, such as thrombo-protection and adequate short-term as well as long-term patency are still in the development and exploration stage. In this study, based on the gas signaling molecule release strategy, SDVGs were prepared by electrospinning using poly(L-lactide-co- ϵ -caprolactone) (PLCL) and gelatin (Gel). Bivalirudin (BVLD) and epigallocatechin gallate-copper (EGCG-Cu) complex were loaded into SDVGs to improve hemocompatibility and nitric oxide (NO) release, respectively. Vascular grafts manifested drug release for up to 40 days *in vitro*; BVLD effectively inhibited thrombosis while the EGCG-Cu complex catalyzed the NO production from endogenous donors (S-nitroso glutathione (GSNO) and glutathione (GSH)), thereby conferring vascular grafts with functions similar to that of the natural vascular endothelium layer. Both *in vitro* and *in vivo* tests demonstrated that SDVGs co-loaded with BVLD and EGCG-Cu (PG-EB) could effectively inhibit thrombosis, alleviate inflammation, and suppress the proliferation of smooth muscle cells (SMCs) while promoting the proliferation of endothelial cells (ECs), and finally regenerate vascular tissues. *In vivo* animal experiments demonstrated that vascular grafts could promote endothelialization and vascular remodeling. In summary, our simultaneous utilization of BVLD and EGCG-Cu may offer a promising avenue for the fabrication of *in situ* regenerable SDVGs.

1. Introduction

In recent years, the incidence of chronic diseases, such as cardiovascular disease (CVD) has been on the rise [1]. Occluded coronary and peripheral arteries are generally treated by the transplantation of autografts, allografts, or artificial synthetic polymer-based vascular grafts [2]. Autologous blood vessels are the clinical gold standard for the treatment of CVD albeit their limited use owing to the different types of

factors, such as less number of donors, additional surgical procedures, and patient health status [3,4]. Poly(ethylene terephthalate) (PET) and expanded polytetrafluoroethylene (ePTFE) have shown satisfactory performance in replacing large-diameter blood vessels (I.D. > 6 mm) albeit their limited success in the reconstruction of small-diameter blood vessels (I.D. < 6 mm) [5]. Synthetic polymer-based vascular grafts have only limited success as small-diameter vessel substitutes, possibly due to the occlusion of the lumen, less blood flow velocity, and intimal

* Corresponding authors.

E-mail addresses: shafiqdr786@yahoo.com (M. Shafiq), xmm@dhu.edu.cn (X. Mo), mailjsc@163.com (S. Jiang), agu43102445@163.com (H. Gu).

¹ G.C., Z.Y., and X.W. are co-first authors.

<https://doi.org/10.1016/j.cej.2024.156555>

hyperplasia (IH). Consequently, the transplanted vascular grafts show poor short-term and long-term patency, thrombosis, and IH [6,7]. Therefore, it is imperative to design alternative biomaterial candidates for the fabrication of small-diameter vascular grafts (SDVGs), which may have salutatory functions alongside the healing potential and *de novo* production of arteries *in vivo*.

Timely vascular endothelialization has an important role in the maintenance of vascular homeostasis and the prevention of vascular diseases. Different types of methods have been proposed to achieve timely endothelialization of SDVGs, such as the incorporation of bioactive molecules, which include vascular endothelial growth factor (VEGF), cell-specific antibodies, and extracellular matrix (ECM) protein-based cell-binding amino acid sequences [8,9]. Before the formation of the endothelium layer, the proliferation and migration of smooth muscle cells (SMCs) into the intima is the main reason for vascular restenosis [10]. While the frequency of restenosis and thrombosis of vascular grafts is greatly reduced after the introduction of anti-proliferative drugs, late thrombosis still remains a persisting dilemma. Moreover, the release of anti-proliferative drugs may inhibit the proliferation and migration of SMCs and may also suppress the proliferation of endothelial cells (ECs), thereby adversely influencing reendothelialization [11]. Recently, different types of gas signaling molecules, such as hydrogen sulfide (H_2S), carbon monoxide (CO), and nitric oxide (NO) have attracted significant attention from the research community in conferring multifunctional characteristics to artificial synthetic vascular grafts including rapid endothelialization, vascular remodeling, and enhanced short-term and long-term patency [12–16]. In native cardiovascular tissues, NO plays multifunctional roles, such as vascular homeostasis, vasoconstriction, vasodilation, endothelium formation, and the proliferation and cell fate regulation of SMCs [17,18]. In addition, NO may inhibit the adhesion and activation of platelets as well as inflammation resolution [19].

S-nitroso serum protein and S-nitroso glutathione are considerably produced in the peripheral circulation [20]. Through catalyzing these endogenous NO donors, a stable release of NO can be attained, thus maintaining vascular homeostasis. Metal ions including copper ions (Cu^{2+}) and ferrous ions (Fe^{2+}) catalyze the production of NO from NO donors. However, ferrous ions (Fe^{2+}) have disadvantages of low catalytic efficiency, unstable nature, and rapid oxidation. Therefore, the current study mainly uses copper ions (Cu^{2+}) to catalyze the production of NO from the donors [21]. Copper (Cu) is an important microelement for the human body; Cu deficiency may cause different types of diseases, such as anemia and CVD. Copper ions (Cu^{2+}) induce VEGF production, which in turn promotes angiogenesis by modulating the hypoxia-inducible factor-1 alpha (HIF-1 α) pathway, thereby facilitating vascular tissue repair [22]. In addition, copper ions (Cu^{2+}) manifest anti-bacterial properties, which may also have implications for anti-inflammation, anti-infection, and tissue repair. Nonetheless, free copper ions (Cu^{2+}) may lead to its higher content in the blood and potential biological toxicity, which necessitate alternative approaches to fully harness the therapeutic potential of copper ions (Cu^{2+}) while avoiding its deleterious toxic effects [23].

EGCG is the most abundant tea polyphenol with a multitude of functions, including anti-inflammatory, anti-bacterial, anti-oxidative, as well as anti-atherosclerotic characteristics [24–26]. For cardiovascular tissue regeneration, EGCG has been shown to protect free radical-induced blood vessel damage as well as regulate the activity of ECs and the phenotype of SMCs in a concentration-dependent manner [25,27]. It has indeed been shown that the function of the tea polyphenols mainly relies on the neighboring phenolic structure to undergo the autoxidation process, which does not excessively rely on the molecular size and conformation [28]. To ascertain the synergistic effect of the EGCG with copper ions (Cu^{2+}), we synthesized the EGCG-Cu complex via coordination of the polyphenol with the copper ions (Cu^{2+}), which may have anti-oxidative, anti-inflammatory, and anti-bacterial effects [29–31]. EGCG-Cu may furnish therapeutic copper ions (Cu^{2+});

the latter may also play an important role in promoting angiogenesis [32]. Li et al. introduced the EGCG-Cu complex into the drug-eluting stents (DES) and reported its salutatory effect on the ECs potentially by scavenging free radicals as well as suppressing overproliferation and migration of SMCs [33].

Since implanted cardiovascular grafts often fail due to platelet adhesion and activation and activation of the coagulation cascade pathway, blood compatibility of vascular grafts also needs to be carefully considered to promote endothelium formation and suppress platelet adhesion and activation [34]. Heparin (Hep) has been widely incorporated into cardiovascular grafts through covalent conjugation or electrostatic immobilization albeit its multiple risks, such as thrombocytopenia, hemophilia, and bleeding. Bivalirudin (BVLD) is the modification of hirudin, which is the direct thrombin inhibitor and can effectively reduce platelet adhesion and activation by suppressing thrombosis [35–37]. Since the binding of the BVLD to thrombin is reversible, it has a much lower risk of bleeding than that of Hep and hirudin [38]. Du et al. showed that the use of BVLD-modified decellularized abdominal aorta was cytocompatible and hemocompatible, and no thrombosis was observed after 3 months of transplantation of SDVGs into the abdominal aorta of rats [39].

Different types of synthetic polymers have been harnessed for the fabrication of SDVGs such as poly(L-lactic acid) (PLLA), poly(ϵ -caprolactone) (PCL), polyglycerol sebacate (PGS), and poly(ester urethane urea) (PEUU) as well as their copolymers. Poly(L-lactide-co- ϵ -caprolactone) (PLCL) is a mechano-elastic, biocompatible, and biodegradable polymer, whose degradability and mechanical properties can be easily tailored by varying the composition between the monomers, architecture (linear, four-armed, star-shaped, etc.), and the degree of polymerization (DP) [40,41]. PLCL may additionally leverage mechanotransduction to regulate the cell phenotype for endothelialization and vascular remodeling [42]. PLCL has been approved by the FDA for clinical use due to its excellent mechanical properties and compliance with natural blood vessels [43]. However, PLCL shows low cytocompatibility due to its high hydrophobicity, which necessitates modification to increase the hydrophilicity as well as the biocompatibility of vascular grafts [44]. Gelatin (Gel) is a water-soluble protein with a relatively low molecular weight, which is easily degradable and has a good affinity with cells as well as biological tissues [45]. Vascular grafts were fabricated by mechano-elastic and biodegradable PLCL and Gel, which are widely used to prepare vascular grafts and other scaffolds for tissue engineering applications [46].

The objective of this research was to delineate the effect of the dual loading of EGCG-Cu and BVLD into PLCL/Gel-based SDVGs. The incorporation of EGCG-Cu and BVLD into vascular grafts is expected to increase the hydrophilicity and enhance biocompatibility via improved cell adhesion (Fig. 1). Hematocompatibility assays and cell culture evaluations indicated that the vascular grafts were able to effectively inhibit the adhesion, activation, and aggregation of platelets, inhibit overproliferation of SMCs while promoting the migration and proliferation of ECs. Taken together, the incorporation of bioactive cues into SDVGs may offer an amenable platform to prevent restenosis while promoting endothelium formation for potential implications for the design of next-generation SDVGs for the treatment of coronary artery disease.

2. Materials and methods

2.1. Materials

Poly(L-Lactide-co- ϵ -caprolactone) (PLCL, LA: CL = 50:50, IV 2.9 dl/g) was acquired from Jinan Daigang Biomaterial Co., Ltd. (Jinan, China). Epigallocatechin gallate (EGCG) and copper chloride dihydrate ($CuCl_2 \cdot 2H_2O$) were acquired from Macklin Biochemical Co., Ltd. (Shanghai, China). Bivalirudin (BVLD) was acquired from Shanghai Yuanye Bio-Technology Co., Ltd. (Shanghai, China). Gelatin (Gel, Type

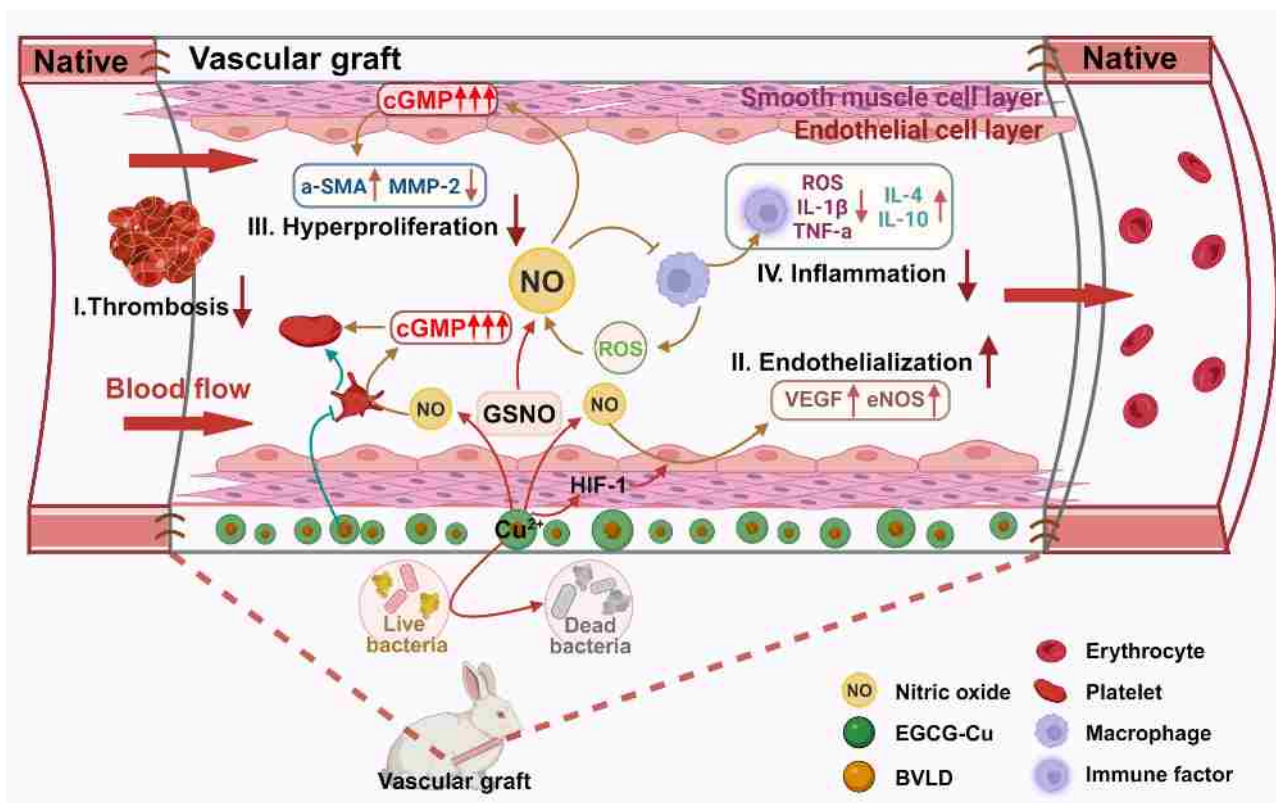


Fig. 1. Schematic illustration of the function of the PG-EB vascular grafts. NO production synergistically inhibited platelet adhesion and macrophage activation and promoted the proliferation of endothelial cells (ECs), while inhibiting the migration and proliferation of smooth muscle cells (SMCs) proliferation and migration. PG-EB vascular grafts significantly improved hemocompatibility, modulated inflammatory responses, promoted endothelialization, and inhibited intimal hyperplasia.

B) was from the porcine and purchased from Sigma-Aldrich Corp. (St. Louis, Missouri, USA). The 1, 1, 1, 3, 3, 3-hexafluoro-2-propanol (HFIP) was obtained from Da-Rui Fine Chemical Co., Ltd. (Shanghai, China). Cell counting kit-8 (CCK-8), 4', 6-diamidino-2-phenylindole (DAPI), dimethyl sulfoxide (DMSO), Cell Trace™ Red CMTPX, and Cell Tracker Green CMFDA were purchased from Yeasen Biotechnology Co., Ltd. (Shanghai, China). S-nitroso glutathione (GSNO) and glutathione (GSH) were obtained from Macklin Biochemical Co., Ltd. (Shanghai, China).

2.2. Sample preparation

2.2.1. Preparation of EGCG-Cu

Epigallocatechin gallate (EGCG) was dissolved in deionized (DI) water and adjusted to the concentration of 0.5 mM (pH = 7.0). Copper (II) chloride dihydrate ($\text{CuCl}_2 \cdot 2\text{H}_2\text{O}$) was dissolved in DI water to obtain a 1 mM solution and added to the EGCG solution. The mixture was reacted at 30 °C for 1 h, filtered, and freeze-dried.

2.2.2. Preparation of spinning solution

EGCG-Cu (0.03 %, w/v) and BVLD (0.02 %, w/v) were dispersed in HFIP. Thereafter, PLCL and Gel (4:1, w/w) were added into the HFIP to obtain the final concentration of 10 % (w/v) and were designated as PG-EB. The PLCL/Gel (PG), the PG + EGCG-Cu (PG-E), and the PG + BVLD (PG-B) were also prepared and used as controls.

2.2.3. Fabrication of electrospun fibers and vascular grafts

The spinning solution was transferred into the 10 mL medical-grade syringe. Fibrous mats were fabricated using the following electrospinning conditions: flow rate, 2 mL/h, spinning needle, 20G, the distance between the spinneret and collector, 15 cm, and the applied voltage, 12 kV. Fibers were collected on the stainless steel collector at a relatively slow rotating speed. The production method of vascular grafts

and membranes was similar, except that the collector for the fabrication of vascular grafts was a stainless steel rod (Φ , 2 mm). Both the membranes and vascular grafts were divided into four groups: *i*) PG, *ii*) PG-B group, *iii*) PG-E group, and *iv*) PG-EB group. The prepared materials were dried in the vacuum oven at room temperature (RT), and sterilized by ultraviolet (UV) light before use.

2.3. Structural analysis

The structural analysis of EGCG-Cu as well as fibers was carried out by the Fourier transform infrared spectroscopy (FTIR, Nicolet iS 10, Thermo Fisher Scientific, USA). The absorption of the characteristic peak of the EGCG-Cu as well as the release kinetics of EGCG-Cu and BVLD were assessed by UV-visible spectrophotometry. The peak absorption and release kinetics of the materials were assessed by UV-visible spectrophotometry. The particle size of EGCG-Cu was measured by Zetasizer Pro (Malvern Panalytical, UK).

The morphology of fibers was examined by scanning electron microscopy (SEM, Phenom, XL, Netherlands) at an accelerating voltage of 5 kV. Image J software was used to analyze the average fiber diameter ($n = 100$). The distribution of elements (C, O, N, and Cu) in the grafts was measured by Energy-dispersive X-ray spectroscopy (EDS, TM-1000, Hitachi, Japan). The surface wettability of the samples was characterized by the water contact angle (WCA, Solon Tech., Shanghai, China). DI water was dropped on samples and captured the images. For WCA, images of water droplets were analyzed by Image J software ($n = 3$). Detail of the degradation of the materials is described in [supporting information](#) (SI. M1. *In vitro* degradation of the materials).

2.4. Mechanical properties

Vascular grafts were immersed in phosphate buffer saline (PBS, pH =

7.4) for 24 h to ensure that the fibers were in a stable state. The length of each tubular sample was fixed at 3 cm, while the inner, as well as outer diameters of vascular grafts, were measured with a vernier caliper. Grafts were positioned within the grips of a uniaxial tensile testing machine (Instron 5567, Norwood, MA) equipped with a 50 N load cell and were analyzed for up to the failure at a crosshead speed of 10 mm/min ($n = 3$).

2.5. NO generation

Vascular grafts (ca. 50 mg, $n = 3$) were immersed in the S-nitroso glutathione (GSNO) solution (50 μM). At pre-determined time points, 50 μL of the solution was collected and transferred into a 96-well plate containing 100 μL of Griess reagent (Sigma-Aldrich Corp., St. Louis, Missouri, USA). Absorbance was recorded at 540 nm by the microplate reader (Multiskan MK3, Thermo, USA). The concentration of NO was measured using the calibration curve prepared by varying concentrations of the sodium nitrite (NaNO_2) solution.

2.6. Blood compatibility

2.6.1. Platelet adhesion assay

For *in vitro* blood compatibility assay of PG-EB, grafts were divided into two groups: *i*) without NO donor (PG-EB (–) group) and *ii*) along with NO donor solution (200 μM GSH and 50 μM GSNO, PG-EB (+) group). The platelet adhesion process is described in SI. (M2. Platelet adhesion). The expression level of cyclic guanosine monophosphate (cGMP) in platelets after incubation with the grafts was determined by the cGMP ELISA kit (Hefei Laier Biotechnology Co., Ltd. Hefei, China).

2.6.2. Blood clotting assay

Electrospun membranes (Φ , 15 mm, $n = 3$) were weighed and placed into a 24-well plate. Recalcified rabbit blood was obtained by mixing 5 mL of fresh anticoagulant rabbit blood with 500 μL of calcium chloride (CaCl_2) solution (0.025 μM), and then 500 μL of Rabbit recalcified whole blood was added into each well. Thereafter, the materials were washed with DI water for 10 min and the filter paper was dried and weighed. The detailed methods of the blood clotting assay and hemolysis rate assay are described in the SI. (M3. Clotting time assay and M4. Hemolysis rate assay).

2.6.3. Anti-thrombogenicity *ex vivo*

Vascular grafts (Φ , 15 mm, $n = 3$) were connected to a catheter, and the whole blood was pumped into vascular grafts by the microcirculatory pump (BT100-2 J, Baoding Longer Pump Co., Ltd., China) *in vitro* for 2 h. Thereafter, vascular grafts were removed and washed with DI water for 10 min. Thrombi were collected, photographed, and analyzed in each sample.

2.7. Biocompatibility assay

2.7.1. Cell culture

The specific procedures for the culture of human umbilical vein endothelial cells (HUVECs), human umbilical artery smooth muscle cells (HUASMCs), and RAW 264.7 macrophages are described in SI. (M5. Cell culture). For *in vitro* cell assays, the PG-EB group was divided into two groups: *i*) without NO donor (PG-EB (–) group) and *ii*) with the donor solution (200 μM GSH and 50 μM GSNO, PG-EB (+) group) in cell culture medium. The NO donor medium was changed every 24 h.

2.7.2. Cell compatibility assay

Electrospun membranes (Φ , 1 cm, $n = 3$) were placed into a 48-well cell culture plate and incubated with 2×10^4 cells. CCK-8 assay and live/dead staining assay were carried out at day 1, 4, and 7. Cell adhesion and morphology were analyzed by SEM.

2.7.3. Cell migration assay

For the Transwell migration assay, inserts along with a polycarbonate membrane (pore size, 8.0 μm , Coring, USA) were placed into 24-well plates and incubated with 1 mL of serum-free medium and 200 μL of extraction solution ($n = 3$). 200 μL of cell suspension (2×10^4 cells/mL) was added into the Transwell inserts. After 12 h, inserts were rinsed with PBS, and cells were fixed with 500 μL of 4 % paraformaldehyde (PFA).

Fixed cells were stained with 500 μL of crystal violet solution (Sigma-Aldrich Corp., St. Louis, Missouri, USA) for 15 min before observing the cells with the microscope (Eclipse TS100, Nikon, Japan). The detailed procedure of the scratch assay is described in SI. (M6. Scratch assay).

2.7.4. HUVECs and HUASMCs co-culture and three-dimensional perfusion culture

The co-culture assay was applied to analyze the effect of the materials on the competitive adhesion of HUVECs and HUASMCs; a detailed procedure is described in SI. (M7. HUVECs and HUASMCs co-culture). Moreover, the detailed method for three-dimensional (3D) perfusion culture is described in SI. (M8. Three-dimensional perfusion culture).

2.7.5. Real-time polymerase chain reaction (RT-PCR)

Total RNA was extracted from cells by the TRLeasy™ Total RNA Extraction Reagent (Yeasen Biotechnology Co., Ltd.). The isolated RNA was reverse transcribed into complementary DNA (cDNA) utilizing the NovoScript® Plus All-in-one 1st Strand cDNA Synthesis SuperMix (Novoprotein Scientific Inc., Suzhou, China). Quantitative RT-PCR was carried out by the NovoStart®SYBR qPCR SuperMix Plus (Novoprotein Scientific Inc.). The relative expression levels of the target genes were calculated by the $2^{-\Delta\Delta\text{Ct}}$ approach ($n = 3$). The target and sequences of primers used for associated genes are shown in Table S1. Glyceraldehyde 3-phosphate dehydrogenase (GAPDH) was used as an internal reference gene.

2.8. Anti-bacterial, anti-oxidative, and anti-inflammatory properties

The anti-bacterial activity of the samples was evaluated with gram-positive bacteria (*Staphylococcus aureus*, *S. aureus*) and gram-negative bacteria (*Escherichia coli*, *E. coli*). The bacteria were cultured in the bacterial cell culture medium (LB Broth) for 24 h. Then 200 μL of bacterial inoculation fluid (10^8 CFU/mL) was added to each sample and incubated for 24 h. The culture solution was taken and diluted, subsequently, 100 μL diluted solution was taken and coated on LB Agar for 12 h. Images were collected by the automated colony counter (Shinese Science & Technology Co., Ltd, Hangzhou, China). Pure bacteria suspension was served as the control group ($n = 3$).

RAW 264.7 macrophages were seeded in the 6-well plate (3×10^5 cells/well). The macrophages were then induced with lipopolysaccharide (LPS, Beijing Solarbio Science&Technology Co., Ltd. Beijing, China) and 1 mL of extract was added after induction. After 24 h, cells were collected for analysis. Cell pellets were resuspended in 100 μL PBS containing 1.25 μg Anti-CD86 antibody and 0.25 μg Anti-CD206 antibody (Abcam, Shanghai, China). Expression of CD86 and CD206 was analyzed using flow cytometry (FACS Calibur, Becton Dickinson, Franklin Lakes, NJ, USA). Detailed methodology for the 2,2-diphenyl-1-picrylhydrazyl (DPPH) assay is provided in SI. (M9. DPPH assay). In addition, intracellular reactive oxygen species (ROS) level was measured by 2,7-dichlorodihydrofluorescein diacetate (DCFH-DA).

2.9. Subcutaneous implantation

All *in vivo* assays were approved by the Shandong Provincial Hospital Affiliated with Shandong First Medical University, Shandong, China (No. 2024080). Sprague-Dawley (SD) rats (female, seven-week-old) were anesthetized with 3 % sodium pentobarbital at the ear margins (dose, 30 mg/kg). Detailed methodology for subcutaneous implantation

is described in SI. (M10. Subcutaneous implantation).

2.10. In vivo assessment

New Zealand white rabbits (weight, 2.5–3.3 kg and age, 5–8 months) were anesthetized with 3 % sodium pentobarbital at the ear margins (dose, 30 mg/kg). Vascular grafts were implanted into the abdominal aorta of rabbits under sterile conditions, as detailed in SI. (M11. *In vivo* assessment). The endothelial coverage of the inner surface of the samples was analyzed by SEM. A detailed process of immunohistochemistry

analysis is described in SI. (M12. Immunohistochemistry analysis).

2.11. Statistical analysis

Data was recorded as mean \pm standard deviation (SD). GraphPad Prism Software Version 8.0 (San Diego, CA, USA) was used for statistical analysis. Statistical comparisons were made by one-way analysis of variance (ANOVA) with Tukey's post-hoc analysis. For all assays, the significance level was set at * $p < 0.05$, ** $p < 0.01$, *** $p < 0.001$.

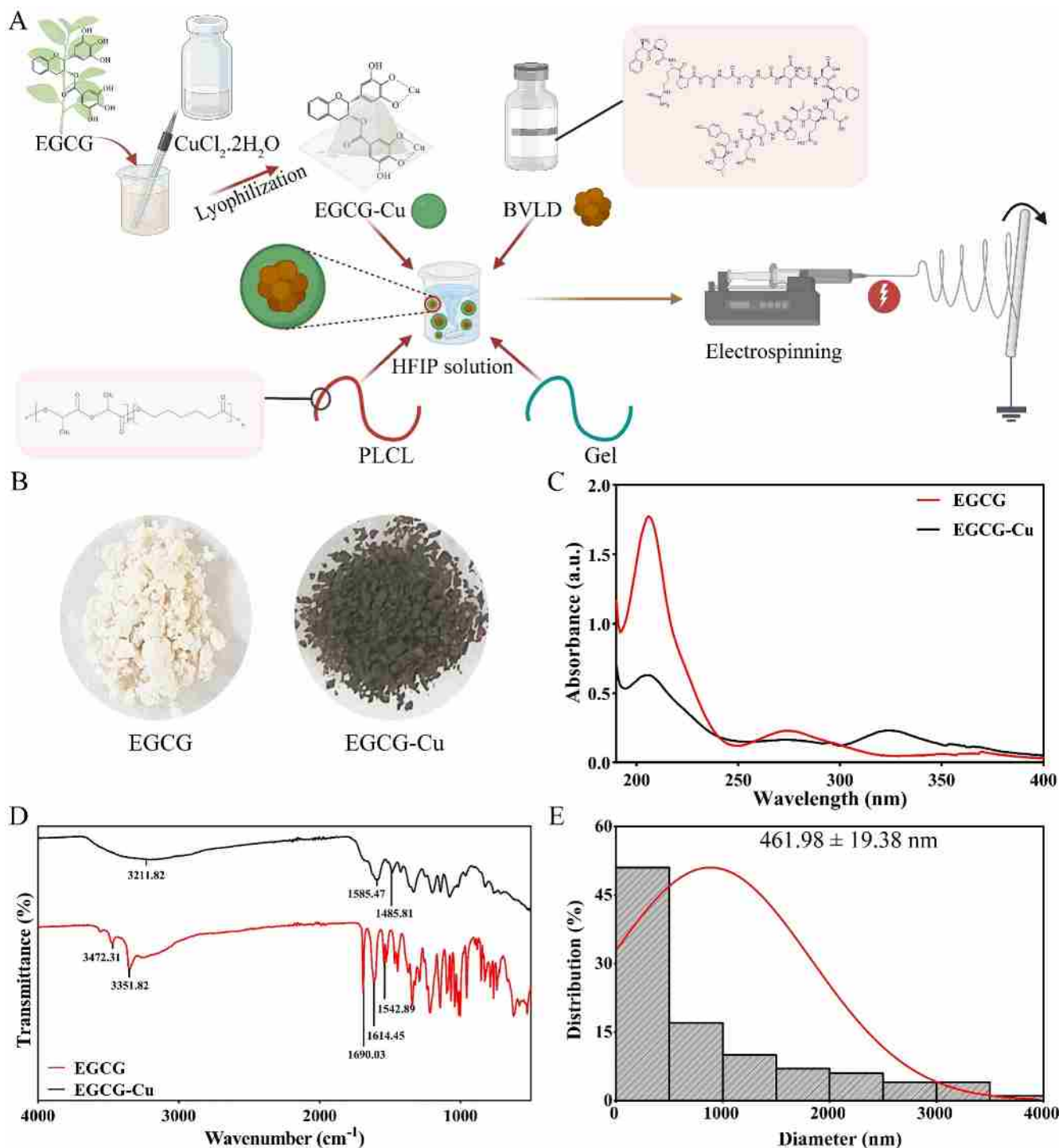


Fig. 2. Synthesis and characterization of EGCG-Cu and fabrication of vascular grafts. (A) Synthesis of EGCG-Cu and preparation of vascular grafts. (B) Images of EGCG and EGCG-Cu. (C) UV-visible absorption spectra of EGCG and EGCG-Cu. (D) ATR-FTIR spectra of EGCG and EGCG-Cu. (E) Diameter distribution of EGCG-Cu.

3. Results

3.1. Characterization of EGCG-Cu

The synthesis process of EGCG-Cu is shown in Fig. 2A. EGCG acted as a ligand, while copper ions (Cu^{2+}) acted as a cross-linker. The gallic acyl group of EGCG provides a chelating site for the complexation of the copper ions (Cu^{2+}), thereby promoting the coordination-driven assembly of EGCG-Cu [32]. The color of EGCG changed significantly from white to brown-black after the formation of coordination complexes with the copper ions (Cu^{2+}) (Fig. 2B). EGCG exhibited a characteristic absorption peak at 275 nm; the characteristic absorption peak of EGCG-Cu appeared at 325 nm (Fig. 2C). The peak shift is ascribed to the fact that part of the phenolic hydroxyl group may form a coordination complex with copper ions (Cu^{2+}), thereby resulting in the change of the overall structure of EGCG [32]. These findings established successful complexation between EGCG and copper ions (Cu^{2+}) to give EGCG-Cu.

FTIR spectra further showed successful complexation between the phenolic hydroxyl group of EGCG and copper ions (Cu^{2+}), which can be described as follows: *i*) During complexation between the phenolic hydroxyl (-OH) groups and copper ions (Cu^{2+}); the latter replaces the hydrogen in the phenolic hydroxyl (-OH) groups to afford O-Cu bond. Moreover, due to the higher polarity of Cu, the electrons of the O atoms on the phenolic hydroxyl (-OH) group become further away, thereby resulting in a reduction in the density of the electron cloud of the whole phenolic hydroxyl (-OH) group. The characteristic absorption peaks of the phenolic hydroxyl (-OH) group appeared in the range of $3,472\text{ cm}^{-1}$

to $3,352\text{ cm}^{-1}$, which were shifted towards lower wave number (e.g., $3,212\text{ cm}^{-1}$), *ii*) The absorption peak of the C = C bond of the benzene ring in EGCG was shifted from $1,614\text{ cm}^{-1}$ to $1,486\text{ cm}^{-1}$ plausibly due to the participation of the phenolic hydroxyl (-OH) group in complexation with the copper ions (Cu^{2+}), and *iii*) EGCG manifested an absorption peak at $1,690\text{ cm}^{-1}$, which was ascribed to the carbonyl (C = O) bond (located in the gallic acyl group), which was shifted to $1,486\text{ cm}^{-1}$ upon complexation with copper ions (Cu^{2+}), thereby further indicating the complexation of the gallic acyl group in EGCG with the copper ions (Cu^{2+}). (Fig. 2D). The average particle size of EGCG-Cu was $461.98 \pm 19.38\text{ nm}$ (Fig. 2E). The above results indicated that EGCG-Cu was successfully synthesized.

3.2. Characterization of vascular grafts

The process of fabrication of SDVGs is shown in Fig. 2A. SDVGs were fabricated by electrospinning (Fig. 3). Vascular grafts manifested a smooth surface and a uniform fiber morphology (Fig. 3B). The average fiber diameter was detected to be $808.96 \pm 248.01\text{ nm}$, $814.97 \pm 214.39\text{ nm}$, $852.52 \pm 233.86\text{ nm}$, and $941.40 \pm 330.69\text{ nm}$ for PG, PG-B, PG-E, and PG-EB groups, respectively (Fig. 3C). While the incorporation of the BVLD and EGCG-Cu increased the fiber diameter, they did not influence the morphology of the randomly oriented fibers (Fig. 3B). All vascular grafts had comparable wall thicknesses without significant differences (Fig. 3D). As shown in Fig. 3E and Fig S1, carbon (C), oxygen (O), nitrogen (N), and copper (Cu) were uniformly distributed into the fibers, which manifested an efficient loading of BVLD and EGCG-Cu into

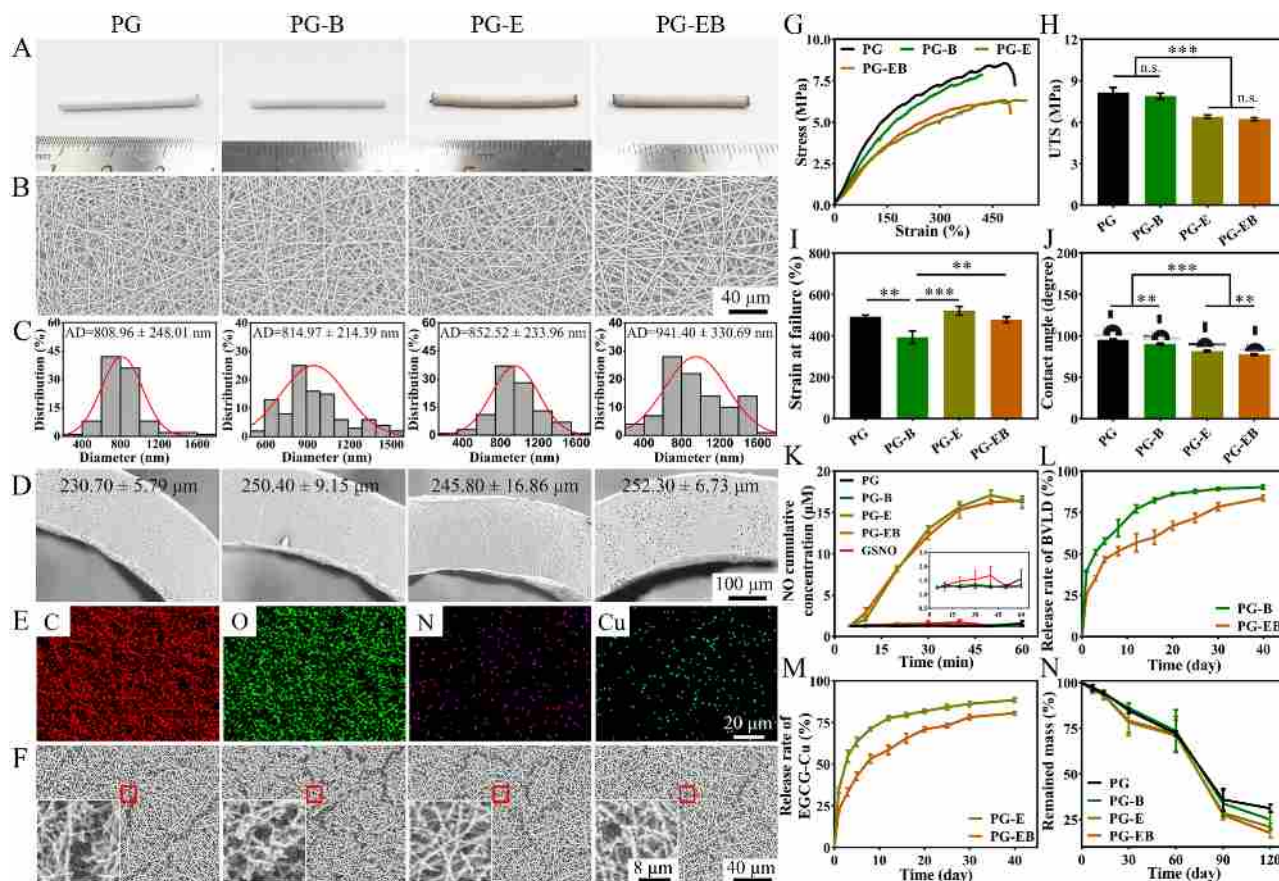


Fig. 3. Characterization of vascular grafts. (A) Images of vascular grafts. (B) SEM micrographs of different types of membranes. Scale bar, 40 μm . (C) Diameter distribution of different types of membranes. (D). SEM micrographs of cross-sections of vascular grafts. Scale bar, 100 μm . (E) EDS analysis of the PG-EB vascular grafts. Scale bar, 20 μm . (F) SEM micrographs of vascular grafts after degradation for up to day 120 *in vitro*. Scale bar, 40 and 8 μm . Representative stress-strain curve (G), UTS (H), strain at failure (I), and the WCA (J) of different types of vascular grafts. (K) The release curve of NP from various vascular grafts. The release of BVLD (L) and EGCG-Cu (M) from grafts. (N) The remained mass after the degradation of vascular grafts *in vitro*.

fibers.

Mechanical properties are a pivotal index for the successful application of vascular grafts; the difference in mechanical properties between the grafts and native vascular tissues may cause a compliance mismatch and potentially intimal hyperplasia (IH) [47]. Therefore, we carried out uniaxial tensile testing to delineate the mechanical properties of vascular grafts under wet conditions. The stress–strain curves of vascular grafts are shown in Fig. 3G. Ultimate tensile strength (UTS) was 8.17 ± 0.3 MPa, 7.90 ± 0.21 MPa, 6.41 ± 0.12 MPa, and 6.23 ± 0.11 MPa for PG, PG-B, PG-E, and PG-EB grafts, respectively (Fig. 3H). Furthermore, the strain at failure values of PG, PG-B, PG-E, and PG-EB grafts were 493.25 ± 7.39 %, 393.51 % ± 30.58 , 521.31 ± 21.38 %, and 477.99 ± 14.37 %, respectively (Fig. 3I). Notably, vascular grafts had higher UTS and strain at failure than that of porcine coronary arteries (UTS: 2.6 MPa and strains at failure: 100 %). [48].

The hydrophilicity/hydrophobicity of vascular grafts was examined by the WCA. The values for the WCA were found to be $95.30 \pm 1.10^\circ$, $90.27 \pm 1.05^\circ$, $81.63 \pm 1.07^\circ$, and $77.47 \pm 0.95^\circ$ for PG, PG-B, PG-E, and PG-EB groups, respectively. Vascular grafts loaded with the BVLD and EGCG-Cu (PG-EB) not only manifested higher strain at failure but also displayed higher hydrophilicity than that of the other groups (Fig. 3J). In addition, *in vitro* NO release assay revealed that both PG-E and PG-EB groups could efficiently catalyze the release of NO from NO donors. Notably, the catalytic rates of PG-E and PG-EB groups did not significantly differ plausibly due to the similar content of EGCG-Cu (Fig. 3K). The stable release rate of NO during vascular implantation contributes to the regeneration of ECs [49].

We next evaluated the cumulative release of BVLD and EGCG-Cu from vascular grafts for up to 40 days *in vitro*. PG-B group showed rapid release of the BVLD at day 1 (released amount, 39.4 ± 0.6 %). The drug release was continued for up to 25 days. At day 25, the cumulative release of BVLD was found to be 87.6 ± 1.2 %, while at day 40, the drug release was found to be 90.3 ± 1.2 %. There was a slight variation in the release of BVLD from day 25 to day 40, indicating that most of the BVLD was released from the SDVGs during the first 25 days. In contrast, the PG-EB group exhibited less drug release than that of the PG-B at day 1 (released amount, 39.4 ± 0.6 % vs. 25.8 ± 0.7 % for PG-B and PG-EB, respectively). The cumulative released amount of the BVLD was found to be 83.8 ± 1.7 % at day 40 (Fig. 3L). The EGCG-Cu also showed release kinetics similar to the BVLD, the PG-EB group could achieve a more sustained release both for the BVLD and EGCG-Cu (Fig. 3M).

One of the key factors in vascular regeneration is the rate of degradation of the implanted materials [46]. During the initial stage of vascular graft implantation, the graft should allow smooth blood flow without a leakage or a rupture. On the other hand, the vascular graft should manifest an appropriate degradation profile commensurate with the neo-tissue regeneration. *In vitro* degradation assay manifested an insignificant morphological change in the fibers by day 30 (Fig. S2). By day 60, the degradation rate of vascular grafts loaded with BVLD and EGCG-Cu was significantly higher in comparison with the PG group (Fig. S2). By day 120, the fibers in all four groups of vascular grafts manifested degradation into smaller fragments (Fig. 3F and Fig. S2). The remained mass of the PG, PG-B, PG-E, and PG-EB grafts was 27.2 ± 4.2 %, 26.7 ± 2.4 %, 20.9 ± 2.1 %, and 18.6 ± 4.1 %, respectively, at day 120 (Fig. 3N). Overall, the degradation rate of PG-E and PG-EB grafts was significantly higher than that of the other groups.

3.3. Blood compatibility

Platelets and coagulation are closely related. When a blood vessel is damaged, platelets rapidly aggregate and attach to the damaged area to form platelet aggregates, thereby suppressing further bleeding [50]. Platelets usually manifest three forms: *i*) circulating platelets exhibiting two sides of slightly concave, oval, or disk-shaped morphology. *ii*) spiny platelets: upon stimulation, platelets extend multiple pseudopods and become dendritic fusing with each other, and *iii*) if the external stimulus

is eliminated in time, spiny platelets can be restored, but dendritic platelets cannot be restored [22]. In the platelet adhesion assay, the anticoagulant properties of the materials were evaluated by assessing the number as well as the morphology of platelets adhering to the materials. The number of platelets adhered to the PG, PG-E, PG-B, PG-EB (–), and PG-EB (+) groups were found to be 33.0 ± 1.0 , 9.3 ± 1.5 , 17.0 ± 2.0 , 6.0 ± 1.0 , and 2.3 ± 0.6 per HPF, respectively (Fig. 4D). The PG group exhibited the highest number of adhered platelets with spiny shape and an activated state. The grafts co-loaded with the BVLD and EGCG-Cu exhibited significantly less number of adhered platelets, which were in an inactivated state (Fig. 4A and 4D).

The concentration of cGMP was significantly increased in the PG-EB (+) group as assessed by ELISA (32.7 ± 2.6 pg/mL, Fig. 4E). The trend for the thrombus weighing assay was found to be similar to that of the platelet adhesion assay. The PG group exhibited significantly higher weight of thrombus (125.7 ± 22.0 mg) than that of the other groups. The BVLD and EGCG-Cu co-loaded grafts did not induce blood clot formation and the thrombus weight was found to be 8.9 ± 1.3 mg (Fig. 4B and 4F). These results suggested that the synergistic effect of BVLD and EGCG-Cu effectively inhibited platelet adhesion alongside reducing thrombus formation.

The coagulation time of the grafts was further analyzed. Since unclotted blood may increase the absorbance of the ultrapure water, less reduction in the absorbance with time change may indicate better fluidity of the blood. The coagulation assay manifested a gradual reduction in the absorbance value of the PG group over time, which is indicative of blood coagulation. Compared to the PG-E group, the absorbance value of the PG-B group decreased slowly. In contrast, the absorbance values of the PG-EB (–) and PG-EB (+) groups did not vary significantly over time, which is suggestive of their good blood compatibility (Fig. 4G).

The anticoagulant properties of the grafts were further revealed by using the APTT assay [22]. APTT values were found to be 31.6 ± 1.5 s, 46.0 ± 3.6 s, 110.0 ± 10.1 s, and 122.3 ± 2.4 s for PG, PG-B, PG-E, and PG-EB groups, respectively (Fig. 4H). The PG-B and PG-EB groups significantly prolonged the clotting time than that of the other groups. The PT results had a similar trend (Fig. 4H). EGCG-Cu may not be directly involved in the coagulation cascade or influence clotting time. Unlike EGCG-Cu, BVLD prolongs clotting time by inhibiting the activation of the endogenous coagulation system [51]. The hemolysis assay revealed an insignificant difference among the groups in terms of hemolysis rate, which was less than 2 % in all groups and was in agreement with the international standard (Fig. 4C and 4I) [52]. These findings revealed that the loading of BVLD and EGCG-Cu effectively improved the blood compatibility of the vascular grafts.

3.4. Ex vivo anti-thrombogenicity assay

The anticoagulation effect of the materials was further evaluated by an *in vitro* whole blood circulation model (Fig. 5A–B). The PG and PG-E groups showed blood vessel occlusion during circulation, and visible thrombi were found within the incised grafts. There was no blockage in the PG-B group and only small blood clots were formed. The PG-EB (–) and PG-EB (+) groups had smooth blood flow and no visible thrombi were formed (Fig. 5C–D). The weight of thrombi was found to be 87.2 ± 9.0 mg, 65.6 ± 7.5 mg, 36.3 ± 3.9 mg, 13.3 ± 1.7 mg, and 8.3 ± 1.1 mg for PG, PG-E, PG-B, PG-EB (–), and PG-EB (+) groups, respectively (Fig. S3). The lumen surface of SDVGs was further analyzed by SEM. The PG group exhibited luminal coverage with the platelets and blood cells, most of which were in an activated state. On the other hand, the PG-B group exhibited significantly less platelet adhesion and activation, erythrocyte aggregation, and fibrin network formation than that of the PG and PG-E vascular grafts. While only a few number of platelets were attached to the PG-EB (–) group, the PG-EB (+) group had the lowest number of adherent blood cells and platelets, which were in an inactivated state (Fig. 5E). These data suggested that PG-EB vascular grafts

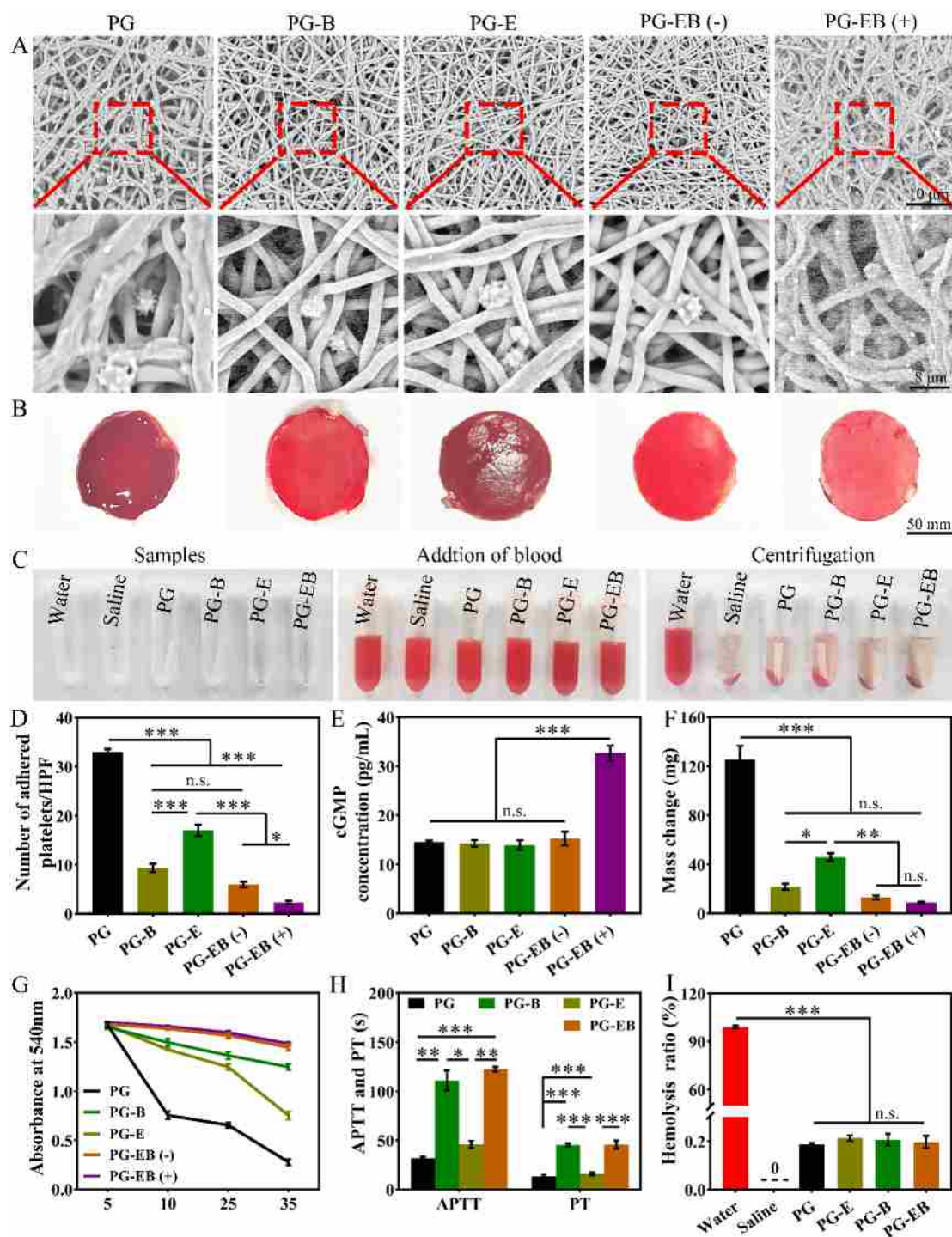


Fig. 4. Blood compatibility of vascular grafts. (A) SEM micrographs of platelet adhesion on the electrospun membranes. Scale bar, 10 μm and 8 μm . (B) Recalcified whole blood formed blood clots on the electrospun membranes. (C) Images of the hemolysis assay of vascular grafts. (D) Quantitative results of platelet adhesion. (E) cGMP expression level of platelets. (F) Quantification of the weight of thrombi on electrospun membranes. (G) Quantification of clotting time in vascular grafts. (H) Quantification of APTT and PT of the plasma of the vascular grafts. (I) Hemolysis rate of vascular grafts.

could suppress thrombus production as well as mimic the function of natural blood vessels.

3.5. Cytocompatibility assay

One of the important factors in achieving good early as well as long-term patency in SDVGs is the formation of the healthy endothelium layer [53]. To delineate the potential for endothelialization of the materials,

HUVECs were cultured on the materials for 1 day, 4 days, and 7 days. As shown in Fig. 6A and S4, at day 1, there was significant adhesion of HUVECs in the PG-EB (+) group. By day 7, the number of HUVECs was gradually increased in each group alongside only a few number of dead cells; the fluorescence intensity of the PG-EB (+) group was significantly higher compared to the other groups (Fig. 6A). CCK-8 assay and SEM micrographs were consistent with the live/dead staining assay (Fig. 6A, 6D, and S4-5). The above results indicated that the PG-EB (+) group

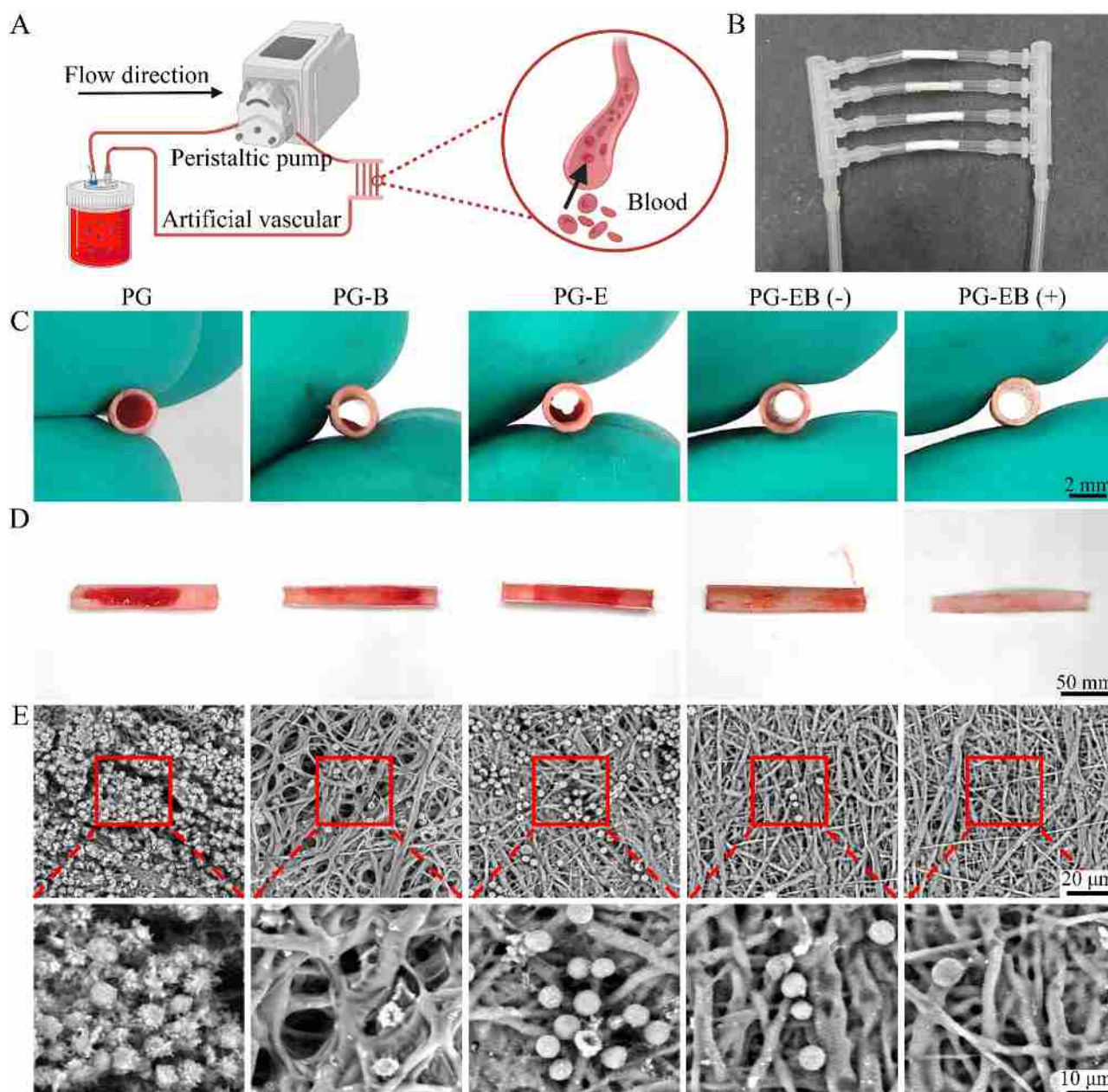


Fig. 5. *In vitro* blood circulation assay. (A) *In vitro* blood circulation model. (B) Image of the perfused vascular grafts. After 2 h of circulation, grafts were observed for thrombus formation in cross-section (C) and lumen (D). Scale bar, 2 mm, and 50 mm. (E) SEM micrographs of the vascular grafts after 2 h of *in vitro* blood circulation. Scale bar, 20 μ m and 10 μ m.

significantly promoted the adhesion and proliferation of HUVECs.

For vascular remodeling process, SMCs should slowly proliferate during the initial phase to form SMCs layer and stop proliferating and migrating thereafter. An overproliferation of SMCs may lead to intimal thickening in the injured vasculature, which may further induce thrombosis and restenosis [54,55]. We therefore screened different groups of vascular grafts for the proliferation of HUASMCs. As shown in Fig. 6B and S6, there was no significant difference among various groups in terms of the adhesion of HUASMCs at day 1. The incorporation of EGCG-Cu inhibited the adhesion as well as the proliferation of HUASMCs, which was further strengthened with the NO production at day 7. The CCK-8 assay as well as SEM micrographs further confirmed the result of live/dead staining of HUASMCs (Fig. 6B, 6E, and S6-7).

We further assessed the selectivity of the materials for cell adhesion by co-culturing HUVECs and HUASMCs. At 4 h, the number of HUVECs

and HUASMCs was almost similar in each group (Fig. S8). At 24 h, the ratio of HUVECs and HUASMCs in PG, PG-E, PG-B, PG-EB (-), and PG-EB (+) groups was 0.86 ± 0.05 , 0.96 ± 0.05 , 1.10 ± 0.10 , 1.23 ± 0.05 , and 1.50 ± 0.10 , respectively (Fig. 6C and 6F). The ratio of HUVECs and HUASMCs was significantly higher in the PG-EB (+) group compared with the other groups, which is indicative of the synergistic effect of EGCG-Cu and NO to selectively enhance the proliferation of HUVECs over HUASMCs, thereby contributing to the formation of the intact single-layer endothelium.

During vascular remodeling, the cell migration rate also directly affects endothelialization [36]. Therefore, we delineated the influence of the different types of material combinations on cell migration using the Transwell migration assay. The number of migrated HUVECs was found to be 703.3 ± 92.9 , 822.7 ± 48.6 , 917.0 ± 76.2 , 1367.0 ± 152.8 , and 2067.0 ± 208.2 per HPF for PG, PG-E, PG-B, PG-EB (-), and PG-EB

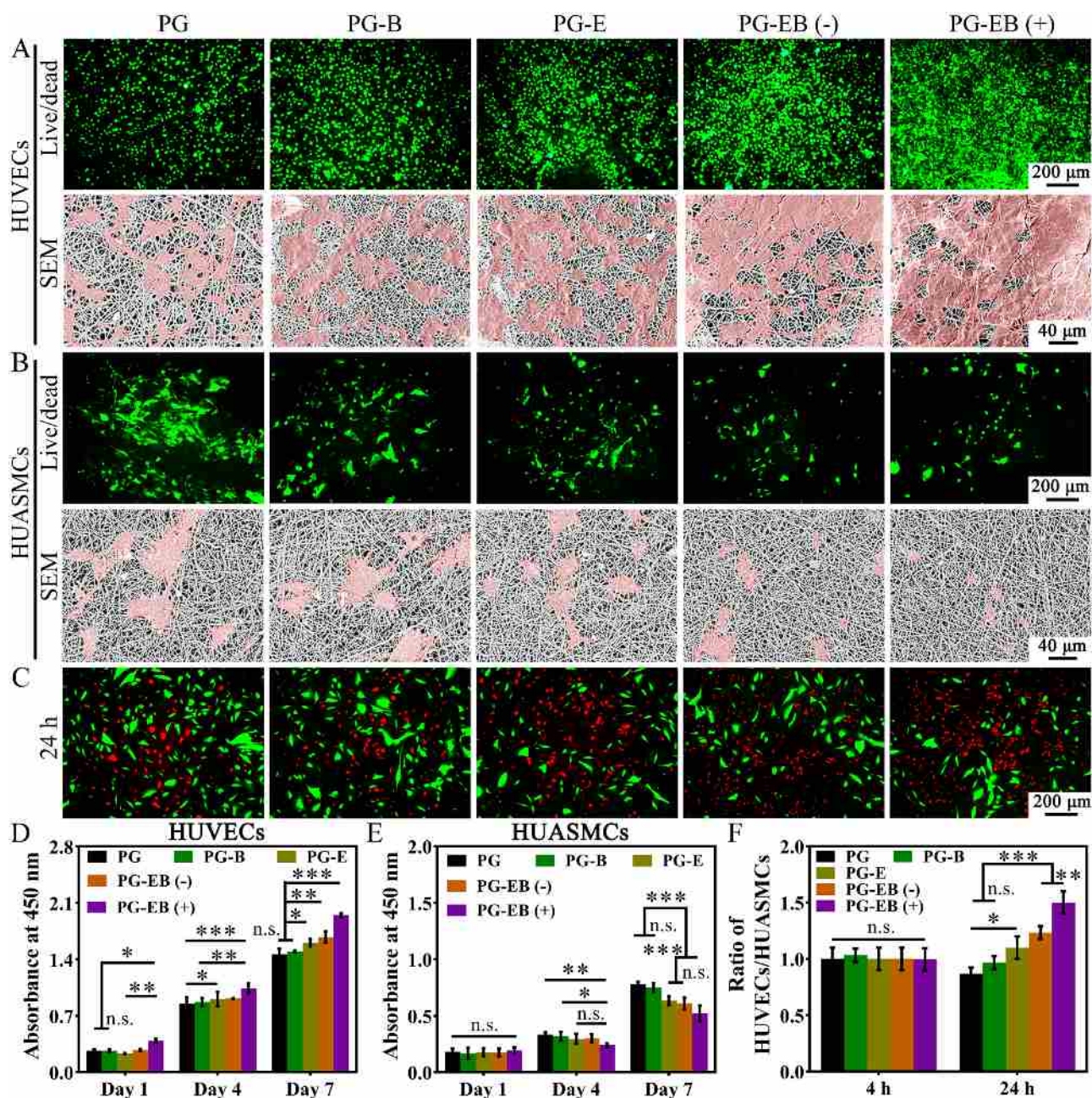


Fig. 6. The cytocompatibility of electrospun membranes. Live/dead staining and SEM micrographs of HUVECs (A) and HUASMCs (B) on electrospun fibers. Permeable live cells were labeled with a green fluorescent dye, and dead cells were labeled with a red dye. Scale bar, 200 μm and 40 μm . (C) HUVECs and HUASMCs co-culture for 24 h (HUVECs: red, HUASMCs: green). Scale bar, 200 μm . HUVECs (D) and HUASMCs (E) proliferation behavior were assessed by CCK-8 assay. (F) Ratio of HUVECs and HUASMCs at 4 h and 24 h. (For interpretation of the references to color in this figure legend, the reader is referred to the web version of this article.)

(+) groups, respectively (Fig. 7A and 7E). The PG-EB (+) group was able to significantly promote the migration of HUVECs. Besides, the migration rate of HUVECs was further characterized by Image J software and found to be $71.7 \pm 5.1\%$, $76.9 \pm 3.3\%$, $78.3 \pm 1.9\%$, $84.8 \pm 2.8\%$, and $93.6 \pm 2.1\%$ for PG, PG-B, PG-E, PG-EB (-), and PG-EB (+) groups, respectively at 24 h (Fig. 7F). The migration rate of HUVECs was significantly higher in both PG-EB (-) and PG-EB (+) groups as compared to the other groups (Fig. 7B and S9). These data indicated that the loading of BVLD and EGCG-Cu could significantly promote the migration of HUVECs; the release of NO could further facilitate the migration of HUVECs.

The total numbers of migrated HUASMCs were found to be 539.0 ± 5.2 , 524.3 ± 23.8 , 491.7 ± 10.4 , 360.0 ± 36.0 , and 180.0 ± 26.4 per

HPF, for PG, PG-E, PG-B, PG-EB (-), and PG-EB (+) groups respectively (Fig. 7C and 7G). The PG-EB (+) group significantly inhibited the migration of HUASMCs as compared to the other groups. The scratch wound healing assay also showed a similar trend to the transwell migration assay of HUASMCs (Fig. 7D, 7H, and S10). These results indicated a synergistic effect between BVLD and EGCG-Cu to suppress the migration of HUASMCs. The cGMP expression level was significantly higher than that of the other groups, with an expression of 30.67 ± 1.40 pg/mL (Fig. 7I).

Cell adhesion and proliferation are often associated with the expression level of specific proteins [56]. VEGF promotes the proliferation and migration of ECs [57], thereby accelerating endothelialization; endothelial nitric oxide synthases (eNOS) produce NO and play

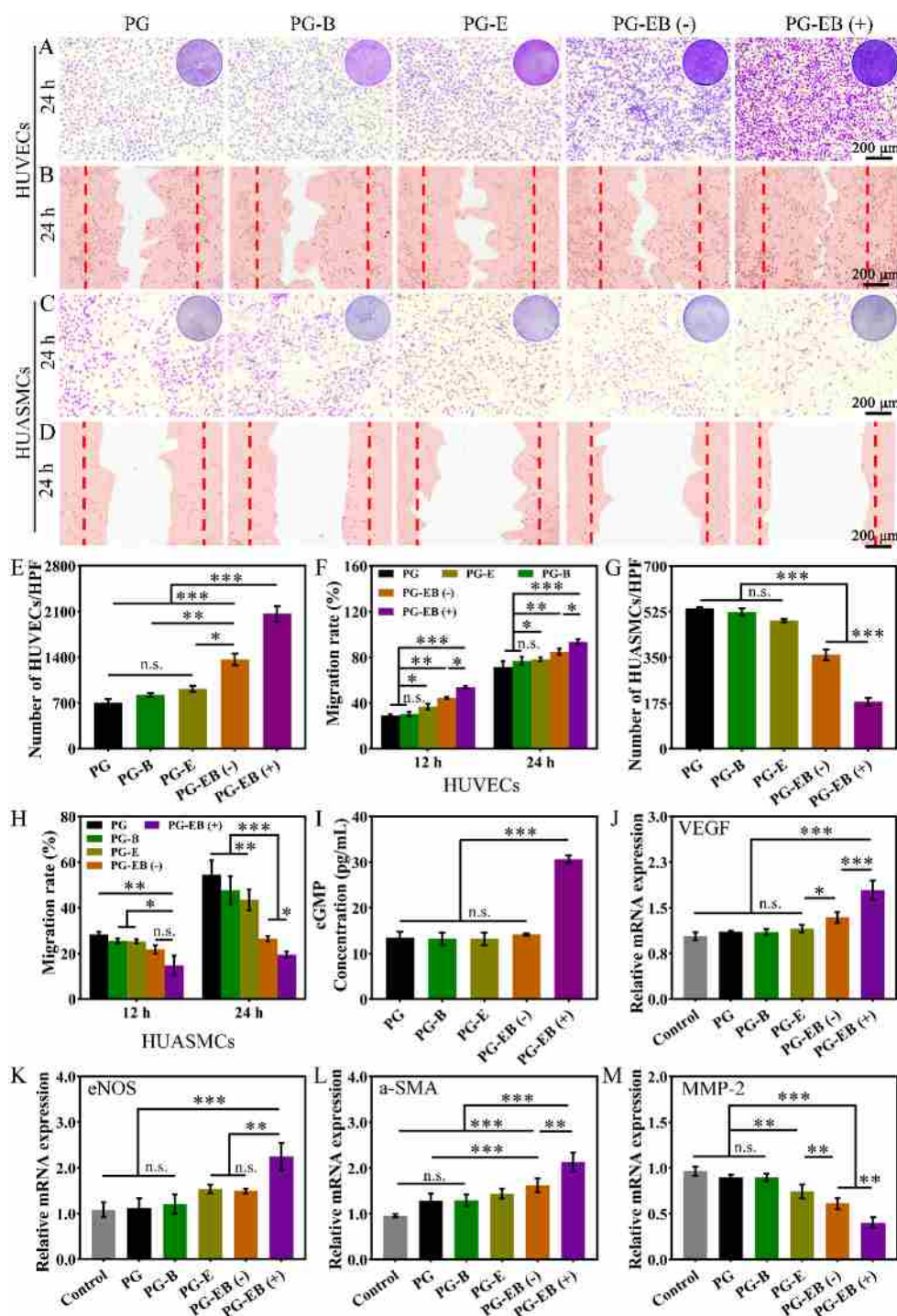


Fig. 7. Biocompatibility of vascular grafts *in vitro*. Transwell migration assay using HUVECs (A) and HUASMCs (C) at 12 h. Scale bar, 200 μ m. Migration of HUVECs (B) and HUASMCs (D) in a scratch wound healing assay at 0 h (the position indicated by the dotted lines) and 24 h. Scale bar, 200 μ m. Quantification of cell migration rates in Transwell migration assays for HUVECs (E) and HUASMCs (G). The migration rate of HUVECs (F) and HUASMCs (H) for 12h and 24h. (I) Quantification of cGMP synthesis in HUASMCs. Quantitative RT-PCR assays showed significant differences between the four groups in the mRNA expression levels of VEGF (J), eNOS (K), α -SMA (L), and MMP-2 (M).

pivotal roles such as the proliferation of ECs, maintenance of vascular tone, and regulation of vascular homeostasis. RT-PCR results indicated that the PG-EB (+) group significantly increased the intracellular expression of VEGF and eNOS than that of the other groups (Fig. 7J and 7K). In addition, the proliferation and migration of SMCs are associated with their phenotype and the changes from contractile-to-synthetic phenotype has been shown to be associated with endothelial

restenosis [58]. Therefore, we employed RT-PCR to detect the expression levels of the contractile phenotype marker, α -SMA, as well as the synthetic phenotype marker, matrix metalloproteinase-2 (MMP-2) in HUASMCs [51,59]. The PG-EB (-) group significantly was able to promote the expression of α -SMA while downregulating the expression of MMP-2 (Fig. 7L-M). The above results indicated that the synergistic effect of BVLD, EGCG-Cu, and NO significantly promoted the proliferation

and migration of HUVECs and maintained the contractile phenotype of HUASMCs.

3.6. Three-dimensional perfusion culture

Adhesion and proliferation of vascular grafts to HUVECs *in vivo* were further simulated by the three-dimensional (3D) perfusion culture system (Fig. 8A). Unlike the static culture of HUVECs to the different types of vascular grafts, only a small number of HUVECs adhered to the various groups of vascular grafts under dynamic culture conditions as evaluated for up to 6 h (Fig. 8B-C, 8E-F), which is ascribed to the shear flow. The numbers of adhered HUVECs were significantly higher in the PG-EB (-) and PG-EB (+) groups compared to the other groups (Fig. 8B-

C, 8E-F), which may be attributed to the incorporation of the hydrophilic drugs; the latter may improve the hydrophilicity of the SDVGs and facilitate cell adhesion. After 5 days of culture, the degree of endothelialization was significantly higher in the PG-EB(+) group than in the other groups (degree of endothelialization: PG, 2.10 ± 0.20 %, PG-B, 51.1 ± 1.3 %, PG-E, 54.5 ± 2.6 %, PG-EB (-), 68.0 ± 6.6 %, PG-EB (+), 91.0 ± 4.3 %, Fig. 8D and 8G), which may be attributed to the release of NO could promote the proliferation of HUVECs. These results manifested that PG-EB vascular grafts could form an intact ECs layer under blood flow shear.

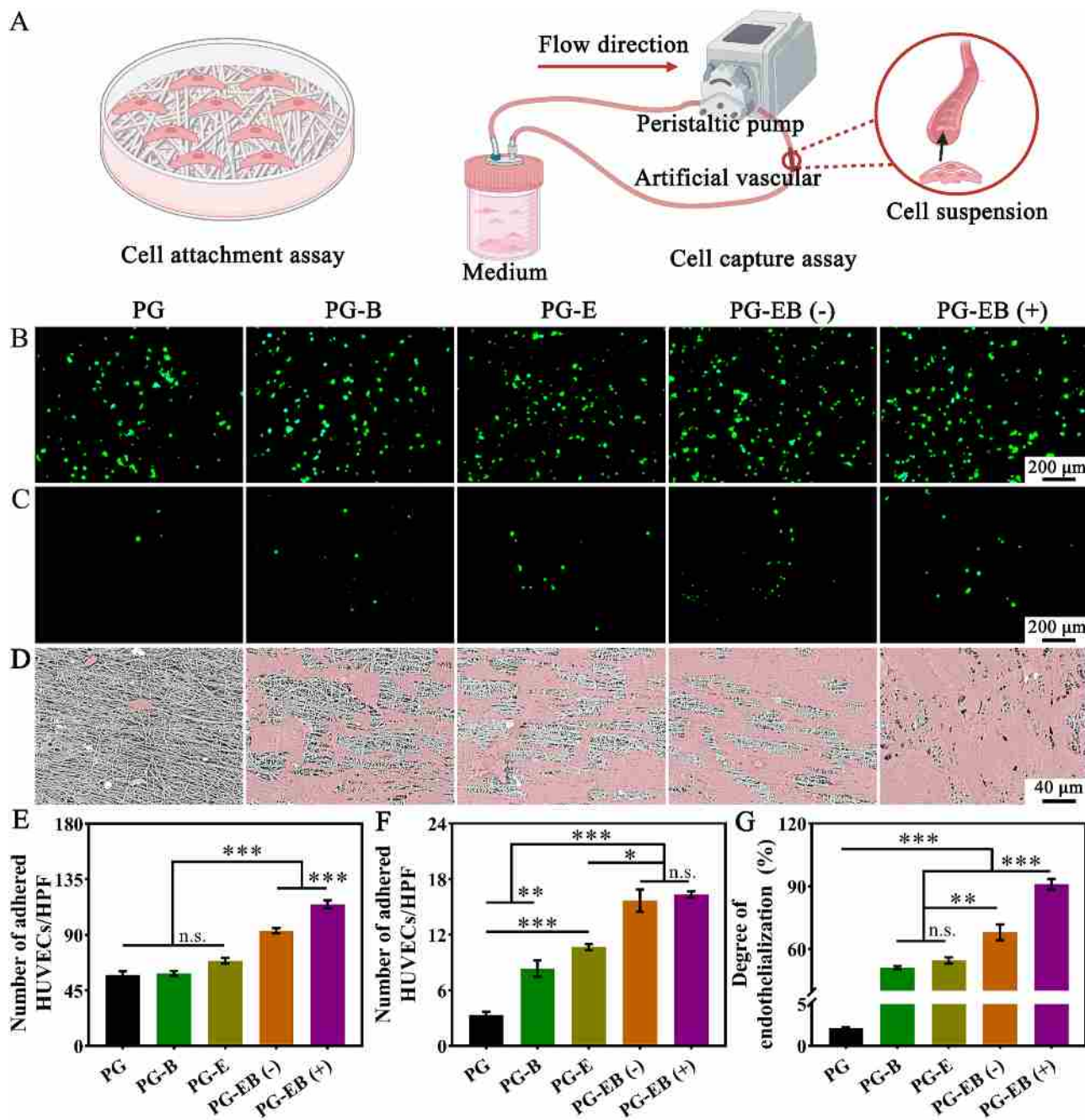


Fig. 8. Three-dimensional perfusion culture of HUVECs with the different types of vascular grafts. (A) Schematic illustration of the 3D perfusion culture system. HUVECs adhesion under static state (B) and shear stress (C). Scale bar, 200 μ m. (D) SEM micrographs of the vascular grafts after three-dimensional perfusion at day 5. Scale bar, 40 μ m. Number of adhered HUVECs per field under static state (E) and shear stress (F). (G) Quantification of the degree of endothelialization.

3.7. Anti-bacterial, anti-oxidative, and anti-inflammatory properties

Most vascular graft infections are caused by bacterial infections, which do not occur at a very high incidence while producing a very high

level of harm [60]. Therefore, we evaluated the anti-bacterial efficacy of the grafts against *E. coli* and *S. aureus*. The PG-E and PG-EB groups significantly inhibited the proliferation of *E. coli* (survival rate of *E. coli*: PG, 82.3 ± 3.0 %, PG-B, 49.3 ± 3.8 %, PG-E, 0.50 ± 0.26 %, PG-EB, 0.11

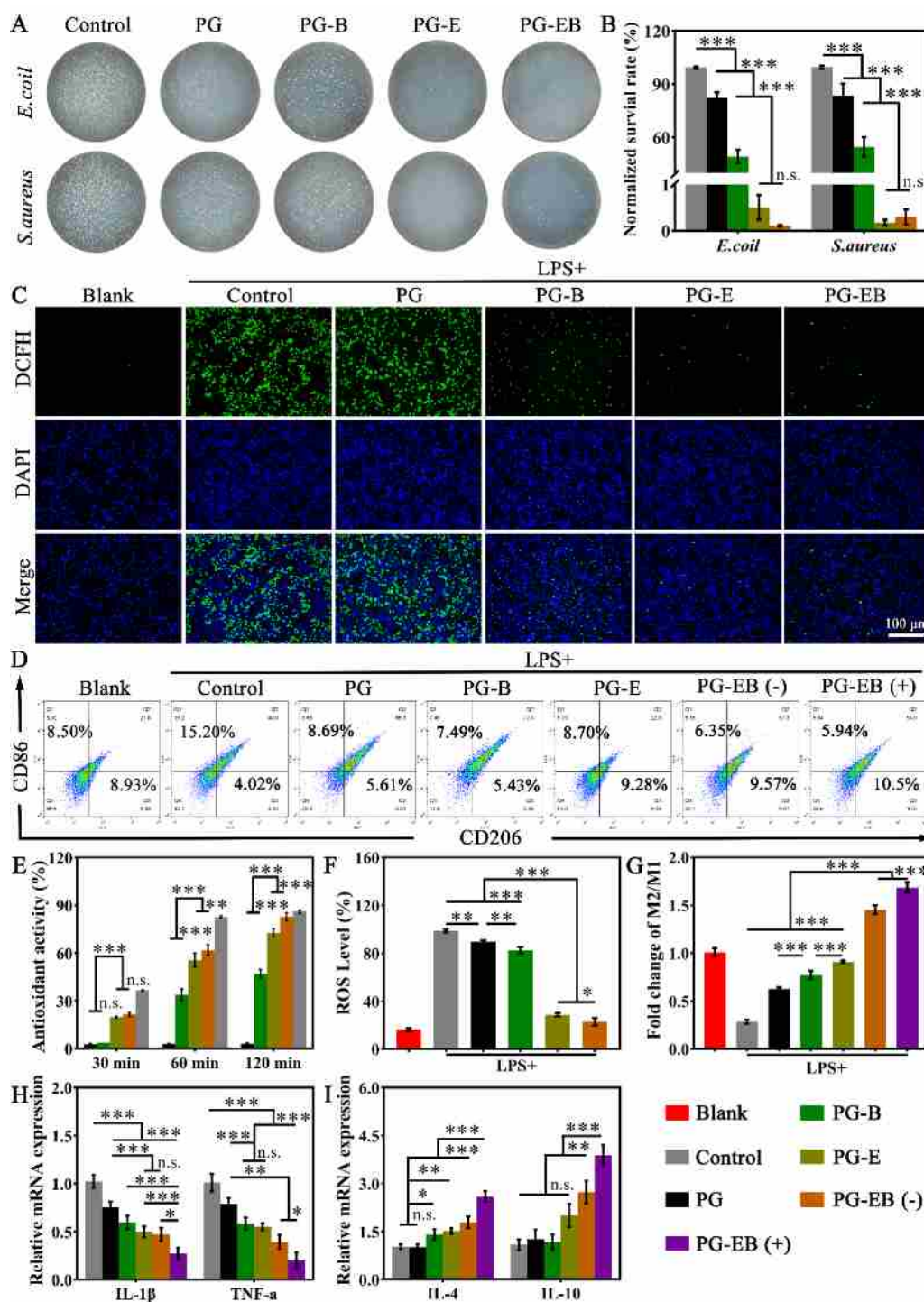


Fig. 9. *In vitro* anti-bacterial, anti-oxidative, and anti-inflammatory assay. (A) Macroscopic images showing the colonies of the *E. coli* (upper row), and *S. aureus* (lower row) grown on broth agar plates after treatment with the electrospun membranes. The survival ratio of *E. coli* and *S. aureus* (B) treated with the different types of membranes. (C) Fluorescence images of RAW 264.7 macrophages stained with DCFH-DA and DAPI after treatment with the conditioned medium at 24 h to detect intracellular ROS-scavenging. Scale bar, 200 μ m. (D) Flow cytometric analysis of M1 macrophage (CD86) and M2 macrophage (CD206) phenotypes. (E) Antioxidative properties of vascular grafts were evaluated by using the DPPH assay. (F) The ROS-scavenging ratio of RAW 264.7 macrophages *in vitro*. (G) Macrophage polarization was studied using the M2/M1 model, and M2/M1 values were determined from flow cytometry results. Quantitative RT-PCR assays showed significant differences between the four groups in the mRNA expression levels of IL-1 β , TNF- α (H), IL-4, and IL-10 (I). Blank, cells without any treatment. Control, cells were incubated with LPS for 24 h. The remained groups of cells were incubated with LPS and respective extracts for 24 h.

$\pm 0.02\%$, vs. control, $99.4 \pm 0.6\%$, Fig. 9A-B). In addition, the survival rate of *S. aureus* in control, PG, PG-E, PG-B, and PG-EB groups were $99.4 \pm 0.8\%$, $83.5 \pm 6.9\%$, $54.7 \pm 5.4\%$, $0.17 \pm 0.06\%$, and $0.30 \pm 0.16\%$, respectively (Fig. 9A-B). These data indicated that the incorporation of the EGCG-Cu may confer anti-bacterial characteristics to the vascular grafts, thereby effectively preventing vascular graft infections.

For vascular remodeling, ROS generated by the inflammatory response not only suppresses the proliferation and migration of ECs, but also inhibits the production of NO, and even causes cell apoptosis [33,61,62]. The anti-oxidative capacity of vascular grafts was assayed by the DPPH test and the DCFH-DA staining. At 30 min, radical scavenging rate (RSR) values were $2.86 \pm 0.07\%$, $3.80 \pm 0.01\%$, $19.8 \pm 0.7\%$, $21.5 \pm 1.2\%$, and $36.6 \pm 0.30\%$ for PG, PG-B, PG-E, PG-EB, and VC groups, respectively. The anti-oxidative capacity of the grafts was further improved over time, probably owing to the gradual release of BVLD and EGCG-Cu. The RSR value of the PG-EB group became almost similar to that of the VC group as earlier as 2 h, thereby indicating its strong anti-oxidative capacity (Fig. 9E). In addition, we assessed intracellular ROS levels by DCFH-DA. Macrophages were stimulated with the LPS to mimic oxidative microenvironment, fluorescent signals were quantified using flow cytometry and fluorescence microscopy. The fluorescence intensity of the PG-B group was weaker as compared to the PG group; the fluorescence intensity was significantly weaker in the PG-E and PG-EB groups (Fig. 9C). Quantitative analysis revealed that the proportion of the FITC-positive channel was significantly lower in the PG-EB group (25.2 ± 0.6), which further confirmed the results of DCFH-DA staining (Fig. 9F). These results indicated significantly higher anti-oxidative capacity of the EGCG-Cu-loaded grafts than that of their counterparts containing BVLD; in the co-loaded vascular grafts, both the EGCG-Cu and BVLD acted synergistically and exhibited significantly higher anti-oxidative properties.

Macrophages are capable of coordinating all phases of blood vessel development: in the early stages of tissue injury and repair, macrophages exhibit a highly pro-inflammatory phenotype (M1). At the latter stages of the tissue injury, the macrophage phenotype changes to an anti-inflammatory or activated macrophage (M2), which promotes vascular tissue repair [63]. Angiogenesis mediated by M2 macrophages has been proven to have a critical role in inflammation resolution and blood vessel regeneration. [64,65] LPS-treated macrophages were found to be activated, which manifested an M2/M1 macrophage ratio of 0.28 ± 0.02 as revealed by flow cytometry. The M2/M1 macrophage ratio was found to be 0.62 ± 0.01 , 0.77 ± 0.04 , 0.91 ± 0.01 , and 1.45 ± 0.04 for PG, PG-B, PG-E, and PG-EB (-) groups, respectively. These results manifested that the synergistic effect of EGCG-Cu and BVLD promoted the polarization of macrophages from the M1 to M2 phenotype. Importantly, the PG-EB (+) group had the highest percentage of M2 macrophages than that of the other groups (Fig. 9D and 9G), suggesting NO release could further promote the breakdown of inflammation.

To further investigate the influence of vascular grafts on macrophage modulation and inflammation resolution, we discerned the gene expression of interleukin 1-beta (IL-1 β), interleukin-4 (IL-4), interleukin-10 (IL-10), and tumor necrosis factor-alpha (TNF-a) by RT-PCR. Pro-inflammatory genes such as (IL-1 β and TNF-a) were found to be significantly increased in LPS-activated macrophages as compared to the other groups. The incorporation of BVLD and EGCG-Cu as well as the production of NO suppressed the production of pro-inflammatory genes (Fig. 9H). Moreover, anti-inflammatory genes including (IL-4 and IL-10) were found to be considerably higher in the EGCG-Cu and BVLD dual-drug loaded groups than in the other groups, suggesting a synergistic anti-inflammatory effect of EGCG-Cu, BVLD, and NO. (Fig. 9I).

3.8. Subcutaneous implantation of vascular grafts in a rat model

To preliminarily evaluate the biocompatibility of vascular grafts, we subcutaneously implanted materials in rats (Fig. S11A). Both the

number of infiltrated cells and the degree of collagen deposition were gradually increased in each group with an increase in the implantation time. At 4 weeks postoperatively, the number of infiltrated cells was significantly higher in the PG-EB group than that of the other groups, which may be attributed to the incorporation of BVLD and EGCG-Cu as well as an increase in the hydrophilicity of the materials (Fig. S11B). Moreover, PG-EB grafts exhibited distinct biodegradation, which may further encourage host cell/tissue infiltration. Masson's trichrome (MT) staining also showed the significant production of collagen in the PG-EB group than that of the other groups (Fig. S11C). The above results suggested that the PG-EB group could enhance cell infiltration, biodegradability, and collagen regeneration.

3.9. Implantation of vascular grafts in a rabbit abdominal aorta model

SDVGs were further implanted as abdominal aorta substitutes in a rabbit model for up to 1 month; the native rabbit blood vessels were used as the control. The PG groups showed occlusion and thrombosis formation. The PG-B group exhibited smooth blood flow with no thrombi deposition, minimal cell adhesion on the luminal side, and infiltration of only a few number of cells from the abluminal side. The lumen of the PG-E group was covered with a layer of cells alongside considerable cellular infiltration from the abluminal side. The PG-EB group was covered with more number of cells on the luminal side as well as abundant cellular infiltration from the abluminal side (Fig. 10A). SEM micrographs further revealed the thrombi deposition in the lumen of the PG group than that of the other groups. While the lumen of the PG-E and PG-EB vascular grafts was mostly covered by the ECs with significant endothelialization, the PG-B group showed less endothelialization (Fig. S12).

The regeneration of vascular grafts was further analyzed by CD31 and α -SMA immunofluorescence (IF) staining. Unlike the PG and PG-B groups, which lacked the regeneration of ECs in the endothelium layer, both the PG-E and PG-EB groups displayed significant regeneration of ECs on the luminal side (Fig. 10B). The PG-EB group exhibited significant regeneration of SMCs as compared to the other groups (Fig. 10C). The above results manifested that PG-EB vascular grafts achieved vascular regeneration. PG-EB grafts also showed less expression of CD68⁺ macrophages plausibly due to the incorporation of BVLD and EGCG-Cu, which may effectively resolve the inflammatory response and polarize macrophages from the M1 to M2 phenotype as observed in our *in vitro* studies (Fig. 10D).

4. Discussion

The natural mature blood vessel consists of three layers, namely the intima, the media, as well as the adventitia [66]. The endothelium layer is in direct contact with the blood environment. ECs attach to the basement membrane along with connective tissues to form the endothelium layer; the latter inhibits platelet adhesion and activation as well as thrombosis, thus maintaining smooth blood flow over time. The medial layer is mainly composed of SMCs and collagen, which confers sufficient mechanical properties to the blood vessels. The adventitia is composed of fibroblasts and loosely structured connective tissue, which can play a key role in the regeneration of injured blood vessels [66,67]. The ideal SDVGs should exhibit sufficient mechanical properties, cytocompatibility, and hemocompatibility [68,69]. Electrospun fibers are morphologically similar to the natural ECM, which can afford a conducive environment for cell adhesion, proliferation, as well as ECM production. Electrospinning has been broadly applied in the preparation of vascular grafts [70–73]. We employed the combination of natural and synthetic copolymers to fabricate SDVGs; PLCL and Gel were used as the components of vascular grafts alongside EGCG-Cu and BVLD to confer multifunctional characteristics to the grafts, including hemocompatibility, anti-oxidative ability, and NO production. A battery of tests manifested that SDVGs co-loaded with EGCG-Cu complex and BVLD (PG-EB) grafts inhibited thrombogenesis and significantly promoted

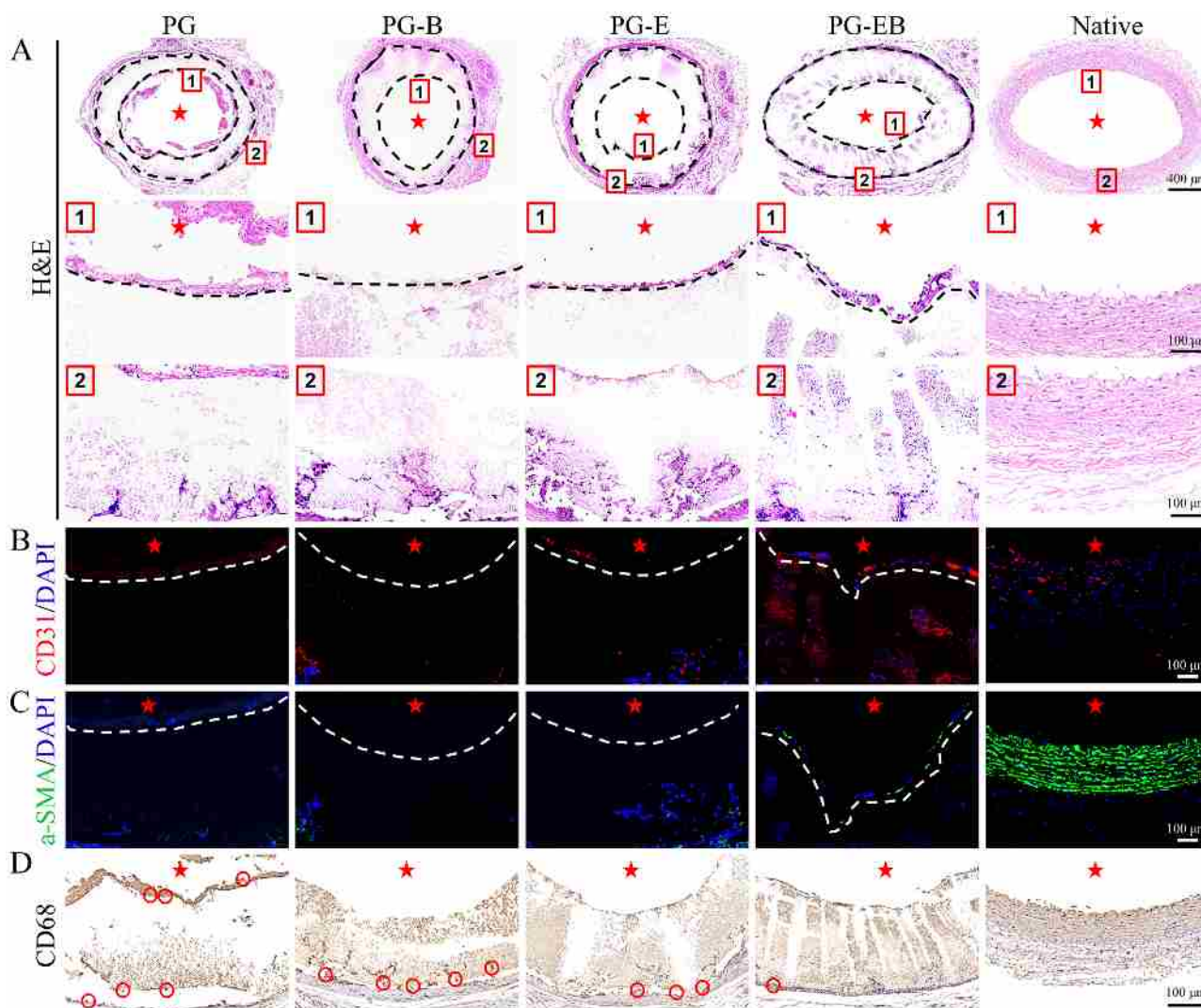


Fig. 10. Transplantation of vascular grafts in an abdominal aorta model in rabbits for up to 1 month. (A) H&E staining. Scale bar, 400 μm and 100 μm . Immunofluorescence staining of the vascular grafts for (B) CD31 (red) and DAPI (blue), and (C) α -SMA (green), and DAPI (blue). (D) Immunohistochemical staining of the vascular grafts for CD68. Scale bar, 100 μm . Image annotations (*) indicate the lumen position. (For interpretation of the references to color in this figure legend, the reader is referred to the web version of this article.)

vascular remodeling.

EGCG-Cu complex is formed by the coordination of the polyphenol EGCG with Cu^{2+} [51], which can effectively load and gradually release BVLD thanks to its porous morphology. BVLD was released in a sustained fashion in the presence of the EGCG-Cu (Fig. 3L). EGCG-Cu and BVLD may also further interact by different types of interactions (e.g., hydrogen bonding, electrostatic interactions, etc.) [32]. The combined loading of the EGCG-Cu and BVLD into vascular grafts afforded the sustained release of the drugs, which may also have implications to improve hemocompatibility as well as induce vascular regeneration. More importantly, drug loading can significantly increase the hydrophilicity of the material (Fig. 3J), which is attributed to i) BVLD, which is comprised of many hydrophilic groups, including the carboxylic ($-\text{COOH}$) group [37], ii) EGCG-Cu is comprised of hydrophilic groups, including the phenolic hydroxyl ($-\text{OH}$) group, which may further increase the hydrophilicity of vascular grafts. Biomaterials with good hydrophilicity can adsorb molecules in the biological environment, such as water molecules and ions, thereby reducing surface tension, increasing wettability, and suppressing irritation to human tissues, which may render them more compatible and close to biological tissues alongside promoting cell adhesion and migration for the subsequent

endothelialization and vascular remodeling [74].

The loading of EGCG-Cu and BVLD not only improved the hydrophilicity of the materials (Fig. 3J) but also accelerated the degradation of the materials and promoted cellular infiltration and collagen deposition (Fig. 3N and S11B-C), which facilitated the remodeling of the ECM and further reduces the risk of calcification formation [75]. The incorporation of EGCG-Cu and BVLD did not influence the mechanical properties of SDVGs and manifested mechanical properties similar to native blood vessels.

Blood-contacting biomaterials are prone to various risks, including thrombosis and hemolysis once they contact the blood [76,77]. The incorporation of EGCG-Cu and BVLD significantly reduced platelet adhesion and activation (Fig. 4C and 4F). It has indeed been previously reported that the EGCG can reduce the concentrations of intracellular calcium by inhibiting the activities of at least two types of enzymes, including spleen tyrosine kinase (Syk) and tyrosine-protein kinase (Lyn). These enzymes prevent the activity of thromboplastin to inhibit platelet aggregation [78]. On the other hand, BVLD inhibits thrombin activity by binding to the catalytically active sites of thrombin, thereby further inhibiting platelet adhesion and activation [37]. Importantly, the EGCG-Cu-loaded material could catalyze the NO production from endogenous

or exogenous NO donors, such as GSNO, thereby affording continuous yet sustained release of NO (Fig. 3K). NO can activate soluble guanylate cyclase to cyclize intracellular guanosine triphosphate (GTP) to cGMP, which activates cGMP-dependent proteases to dephosphorylate myosin light chains, thereby inhibiting platelet adhesion and activation [55,79,80]. Thus, after incorporation of the NO donor solution, the cGMP expression level was significantly increased in the PG-EB group, which could effectively reduce platelet adhesion and thus inhibit thrombosis (Fig. 4A-B, 4E, and 5C-E).

ECs play a key role in regulating thrombosis, the proliferation of SMCs, as well as modulation of inflammatory response [22,81]. Thus, endothelialization is essential both for the short-term and long-term patency of vascular grafts. EGCG-Cu may act as an anti-oxidative agent and can scavenge free radicals and potentially the as well as by additional pathways (Fig. 9C, and 9E-F), thereby protecting oxidative stress-mediated damage of ECs. It has been previously shown that the EGCG can inhibit ROS-induced apoptosis in ECs, promote the expression of B-cell lymphoma-2 (Bcl-2) protein, suppress the expression of BCL2-Associated X (Bax) protein, as well as reduce the cleavage and activation of Caspase-3 [82]. Thus, the incorporation of EGCG-Cu into vascular grafts was able to promote the proliferation of HUVECs. Moreover, NO produced in the PG-EB (+) group could further promote the proliferation of HUVECs. Consequently, the PG-EB (+) group showed higher cell viability, cell proliferation, and cell migration than that of the other groups as assessed by using HUVECs (Fig. 6D, and S4-5).

Intimal hyperplasia (IH) is caused by the abnormal proliferation of SMCs, which ultimately leads to vascular restenosis [51]. Zhang et al. introduced EGCG-Cu as an anti-proliferative drug into the drug-eluting stents (DES), which significantly inhibited the proliferation and migration of SMCs [32]. EGCG-Cu was able to inhibit the proliferation and migration of HUASMCs (Fig. 6E, and S6-7). The inhibitory effect of the PG-EB (+) group on the proliferation of HUASMCs was further strengthened because the PG-EB (+) group released NO, which may regulate vasodilation and contraction through the cGMP pathway and suppress the migration and proliferation of SMCs [20]. While EGCG-Cu could suppress the proliferation of SMCs, only PG-EB vascular grafts showed the expression of CD31 and α -SMA, and all other groups lacked the expression of α -SMA at 1 month (Fig. 10B-C), which is suggestive of the ability of PG-EB vascular grafts to achieve regeneration of SMCs and vascular remodeling and may further regulate endothelialization [83].

The inflammatory response may also cause restenosis [84]. The occurrence and progression of inflammation are closely linked to the pro-inflammatory (M1) and anti-inflammatory (M2) macrophages. M1 macrophages mainly stimulate and maintain inflammation and produce pro-inflammatory cytokines (e.g., IL-1 β and TNF- α); conversely, M2 macrophages participate in the regulation as well as resolution of inflammation, generate anti-inflammatory cytokines, such as IL-4 and IL-10, facilitate tissue repair as well as maintain immune homeostasis [85,86]. The loading of BVLD and EGCG-Cu not only promoted the polarization of macrophages from M1 to M2 phenotypes but also significantly inhibited the generation of inflammatory cytokines (Fig. 9D, and 9G-H). The release of NO also conferred anti-inflammatory characteristics to the vascular grafts (Fig. 9D). Moreover, PG-EB vascular grafts reduced the expression of CD68 as well as effectively attenuated the persistent inflammatory response; the mild cellular inflammation and tissue response instead facilitated the healing of injured blood vessels and tissues [87].

This study also has several limitations: i) Vascular grafts have shorter graft lengths, which were only implanted for up to 1 month. This short-term implantation of vascular grafts may not be sufficient to clearly delineate the endothelialization mechanisms relevant to humans. ii) In this study, we used animals that were healthy and young, and the ability to regenerate tissues may vary between age groups. Different stages of animal development significantly affect the ability to regenerate tissue, and studies have shown that the success of clinical trials of vascular grafts is more pronounced in pediatric patients than in adult patients

[88]. Therefore, further studies will focus on the length and diameter of vascular grafts for potential transplantation in a large animal model alongside implantation for a longer time period and an in-depth evaluation of endothelialization and vascular remodeling. Nevertheless, these polyphenol-based SDVGs mimicked the function of native endothelium. *In vitro* and *in vivo* animal experiments demonstrated that the incorporation of EGCG-Cu and BVLD significantly improved the hemocompatibility, reendothelialization, and vascular remodeling alongside conferring additional anti-oxidative, anti-inflammatory, and anti-bacterial characteristics to the vascular grafts. Taken together, our approach of simultaneously harnessing BVLD and EGCG-Cu to improve the performance of artificial synthetic vascular grafts may be worthy for future research investigations and may also have broad implications for the scaffold materials used for other bio-related applications.

5. Conclusions

Our study utilized electrospinning to fabricate the PG-EB vascular grafts, which could mimic the release of NO from natural ECs to suppress platelet activation and adhesion, thus inhibiting thrombosis and early restenosis. The sustained release of NO also effectively promoted the proliferation of ECs as well as inhibited the overproliferation of SMCs, which promoted the regeneration of vascular tissue at an early stage and prevented the development of restenosis at a later stage. At the same time, the polyphenol EGCG-Cu effectively scavenged oxidants, thus preventing oxidative stress damage. It also inhibited inflammatory cell activation and expression of inflammatory genes (IL-1 β and TNF- α). Moreover, the anti-bacterial properties of SDVGs were effective in reducing the likelihood of infection during the procedure.

In vivo vascular implantation further confirmed that the combination of hydrophilic EGCG-Cu and NO could effectively inhibit restenosis of vascular grafts while promoting rapid endothelialization. The above result indicated that normal reconstruction of blood vessels could be achieved by mimicking the release of gas signaling molecules, which provided a new approach to designing SDVGs.

CRedit authorship contribution statement

Guangfang Cai: Writing – original draft, Investigation, Formal analysis. **Zhengchao Yuan:** Writing – review & editing, Methodology, Investigation. **Xinyi Wang:** Investigation, Formal analysis. **Siyuan Wu:** Resources, Methodology, Investigation. **Shasha Zhou:** Software, Resources, Methodology. **Zheng Lei:** Validation, Software, Funding acquisition. **Peng Li:** Investigation, Data curation. **Mohamed EL-Newehy:** Validation, Supervision. **Meera Moydeen Abdulhameed:** Resources, Methodology, Investigation. **Muhammad Shafiq:** Writing – review & editing, Supervision, Formal analysis, Methodology, Writing – original draft. **Xiumei Mo:** Writing – review & editing. **Shichao Jiang:** Writing – review & editing, Resources, Methodology. **Hongbing Gu:** Writing – review & editing, Supervision.

Declaration of competing interest

The authors declare that they have no known competing financial interests or personal relationships that could have appeared to influence the work reported in this paper.

Acknowledgments

The project was supported by the Songjiang District Committee of Science and Technology, Shanghai, China (Grant No.2023SJKWGG040), Science and Technology Commission of Shanghai Municipality, China (20DZ2254900), Sino German Science Foundation Research Exchange Center, China (M-0263), and China Education Association for International Exchange (2022181). This project was supported by Researchers Supporting Project Number (RSP2024R65), King Saud University,

Riyadh, Saudi Arabia. This project was also supported by the Taishan Scholars Program of Shandong Province (tsqn201812141), Shandong Provincial Natural Science Foundation (ZR2021MH004).

Appendix A. Supplementary data

Supplementary data to this article can be found online at <https://doi.org/10.1016/j.cej.2024.156555>.

Data availability

The data that has been used is confidential.

References

- S. Cheng, C. Hang, L. Ding, L. Jia, L. Tang, L. Mou, J. Qi, R. Dong, W. Zheng, Y. Zhang, X. Jiang, Electronic blood vessel, *Matter* 3 (5) (2020) 1664–1684, <https://doi.org/10.1016/j.matt.2020.08.029>.
- S. Pashneh-Tala, S. MacNeil, F. Claeysens, The tissue-engineered vascular graft—past, present, and future, *Tissue Eng. Part B Rev.* 22 (1) (2015) 68–100, <https://doi.org/10.1089/ten.teb.2015.0100>.
- F.O. Obiweluozor, G.A. Emechebe, D.-W. Kim, H.-J. Cho, C.H. Park, C.S. Kim, I. S. Jeong, Considerations in the development of small-diameter vascular graft as an alternative for bypass and reconstructive surgeries: a review, *Cardiovasc. Eng. Technol.* 11 (5) (2020) 495–521, <https://doi.org/10.1007/s13239-020-00482-y>.
- H. Kuang, Y. Wang, J. Hu, C. Wang, S. Lu, X.J.A.A.M.I. Mo, A method for preparation of an internal layer of artificial vascular graft co-modified with Salvanolic acid B and heparin, *ACS Appl. Mater. Interfaces* 10(23) (2018) 19365–19372. Doi: 10.1021/acsami.8b02602.
- W.E. King, G.L. Bowlin, Near-field electrospinning of polydioxanone small diameter vascular graft scaffolds, *Mech. Behav. Biomed. Mater.* 130 (2022) 105207, <https://doi.org/10.1016/j.jmbbm.2022.105207>.
- L. Bordenave, P. Menu, C. Baquey, Developments towards tissue-engineered, small-diameter arterial substitutes, *Expert Rev. Med. Devices* 5 (3) (2008) 337–347, <https://doi.org/10.1586/17434440.5.3.337>.
- C. Zhang, R. Cha, C. Wang, X. Chen, Z. Li, Q. Xie, L. Jia, Y. Sun, Z. Hu, L. Zhang, F. Zhou, Y. Zhang, X. Jiang, Red blood cell membrane-functionalized nanofibrous tubes for small-diameter vascular grafts, *Biomaterials* 297 (2023) 122124, <https://doi.org/10.1016/j.biomaterials.2023.122124>.
- S. Kang, Y.J. Chi, K. Cho, H.J. Lee, W.-G. Koh, Dual surface modification of poly(L-lactide) scaffold achieved by thermal incorporation of aligned nanofiber and click immobilization of VEGF to enhance endothelialization and blood compatibility, *Appl. Surf. Sci.* 589 (2022) 152969, <https://doi.org/10.1016/j.apsusc.2022.152969>.
- Q. Zhang, S. Duncan, D.A. Szulc, C. de Mestral, M.J.B. Kutryk, Development of a universal, oriented antibody immobilization method to functionalize vascular prostheses for enhanced endothelialization for potential clinical application, *J. Biol. Eng.* 17 (1) (2023) 37, <https://doi.org/10.1186/s13036-023-00356-6>.
- Y. Fan, J. Pei, Y. Qin, H. Du, X. Qu, W. Li, B. Huang, J. Tan, Y. Liu, G. Li, M. Ke, Y. Xu, C. Zhu, Construction of tissue-engineered vascular grafts with enhanced patency by integrating heparin, cell-adhesive peptide, and carbon monoxide nanogenerators into acellular blood vessels, *Bioact. Mater.* 34 (2024) 221–236, <https://doi.org/10.1016/j.bioactmat.2023.12.015>.
- Y. Kang, Y. Cai, W. Pan, Rapamycin and paclitaxel affect human aortic smooth muscle cells-derived foam cells viability and proliferation, *Braz. J. Cardiovasc. Surg.* 37 (2) (2022) 200–206, <https://doi.org/10.21470/1678-9741-2020-0179>.
- F. Liang, D. Jin, L. Wang, J. Zhang, P. Li, J. Yuan, Y. Pan, M. Yin, A small-diameter vascular graft promotes rapid and benign remodeling of the neointima through dual release of nitric oxide and hydrogen sulfide, *Compos. Part B: Eng.* 272 (2024) 111172, <https://doi.org/10.1016/j.compositesb.2023.111172>.
- P. Li, F. Liang, L. Wang, D. Jin, Y. Shang, X. Liu, J. Zhang, Y. Sun, Y. Pan, J. Yuan, J. Shen, M. Yin, Corrigendum to “bilayer small-diameter vascular grafts with on-demand NO and H(2)S release capabilities”, *Bioact. Mater.* 33 (2024) 69–70, <https://doi.org/10.1016/j.bioactmat.2023.10.029>.
- L. Wang, C. Miao, F. Liang, Y. Shang, Y. Sun, J. Zhang, J. Shen, M. Yin, J. Yuan, Hydrogen sulfide releasing and carboxybetaine modified vascular graft with enhanced anticoagulant, anticalcification, and pro-endothelialization properties, *Appl. Mater. Today* 35 (2023) 101976, <https://doi.org/10.1016/j.apmt.2023.101976>.
- P. Li, D. Jin, J. Dou, L. Wang, Y. Wang, X. Jin, X. Han, I.-K. Kang, J. Yuan, J. Shen, M. Yin, Nitric oxide-releasing poly(ϵ -caprolactone)/S-nitrosylated keratin biocomposite scaffolds for potential small-diameter vascular grafts, *Int. J. Biol. Macromol.* 189 (2021) 516–527, <https://doi.org/10.1016/j.ijbiomac.2021.08.147>.
- L. Wang, F. Liang, Y. Shang, X. Liu, M. Yin, J. Shen, J. Yuan, Endothelium-mimicking bilayer vascular grafts with dual-releasing of NO/H₂S for anti-inflammation and anticalcification, *ACS Appl. Mater. Interfaces* 16 (1) (2024) 318–331, <https://doi.org/10.1021/acsami.3c15176>.
- B.E. Laursen, E. Stankevicius, H. Pilegaard, M. Mulvany, U. Simonsen, Potential protective properties of a stable, slow-releasing nitric oxide donor, *GEA* 3175, in the lung, *Cardiovasc. Drug Rev.* 24 (3–4) (2006) 247–260, <https://doi.org/10.1111/j.1527-3466.2006.00247.x>.
- D.A. Riccio, M.H. Schoenfisch, Nitric oxide release: part I. macromolecular scaffolds, *Chem. Soc. Rev.* 41(10) (2012) 3731–41. Doi: 10.1039/c2cs15272j.
- T.A. Tabish, M.J. Crabtree, H.E. Townley, P.G. Winyard, C.A. Lygate, Nitric oxide releasing nanomaterials for cardiovascular applications, *JACC Basic Transl. Sci.* 9 (5) (2024) 691–709, <https://doi.org/10.1016/j.jacbts.2023.07.017>.
- Z. Yang, Y. Yang, K. Xiong, X. Li, P. Qi, Q. Tu, F. Jing, Y. Weng, J. Wang, N. Huang, Nitric oxide producing coating mimicking endothelium function for multifunctional vascular stents, *Biomaterials* 63 (2015) 80–92, <https://doi.org/10.1016/j.biomaterials.2015.06.016>.
- N. Lyu, Z. Du, H. Qiu, P. Gao, Q. Yao, K. Xiong, Q. Tu, X. Li, B. Chen, M. Wang, G. Pan, N. Huang, Z. Yang, Mimicking the nitric oxide-releasing and glycoalkaloid functions of endothelium on vascular stent surfaces, *Adv. Sci. (weinh)* 7 (21) (2020) 2002330, <https://doi.org/10.1002/adv.202002330>.
- H. Xu, Z. Liu, Y. Wei, Y. Hu, L. Zhao, L. Wang, Z. Liang, X. Lian, W. Chen, J. Wang, Z. Yu, X. Ma, D. Huang, Complexation-induced resolution enhancement pleiotropic small diameter vascular constructs with superior antibacterial and angiogenesis properties, *Adv. Healthc. Mater.* 12 (29) (2023) 2301809, <https://doi.org/10.1002/adhm.202301809>.
- L. Wang, F. Liang, Y. Shang, X. Liu, M. Yin, J. Shen, J. Yuan, Endothelium-mimicking bilayer vascular grafts with dual-releasing of NO/H(2)S for anti-inflammation and anticalcification, *ACS Appl. Mater. Interfaces* 16 (1) (2024) 318–331, <https://doi.org/10.1021/acsami.3c15176>.
- J. Qu, H. Pei, X.Z. Li, Y. Li, J.M. Chen, M. Zhang, Z.Q. Lu, Erythrocyte membrane biomimetic EGCG nanoparticles attenuate renal injury induced by diquat through the NF- κ B/NLRP3 inflammasome pathway, *Front. Pharmacol.* 15 (2024) 1414918, <https://doi.org/10.3389/fphar.2024.1414918>.
- K. Ismiyatin, T. Yuanita, W. Saraswati, M.R. Saptaningrum, D.C. Putri, R. A. Miranda, B.A. Wibowo, Mixing ratio of nano hydroxyapatite and Epigallocatechin-3-gallate (EGCG) towards viscosity and antibacterial effect as a potential pulp capping material: an experimental study, *Saudi Dent. J.* 36 (7) (2024) 1006–1009, <https://doi.org/10.1016/j.sdentj.2024.04.009>.
- Y. Liu, Y. Long, J. Fang, G. Liu, Advances in the anti-atherosclerotic mechanisms of epigallocatechin gallate, *Nutrients* 16 (13) (2024), <https://doi.org/10.3390/nu16132074>.
- M. Shafiq, Y. Chen, R. Hashim, C. He, X. Mo, X. Zhou, Reactive oxygen species-based biomaterials for regenerative medicine and tissue engineering applications, *Front. Bioeng. Biotechnol.* 9 (2021) 821288, <https://doi.org/10.3389/fbioe.2021.821288>.
- D.G. Nagle, D. Ferreira, Y.D. Zhou, Epigallocatechin-3-gallate (EGCG): chemical and biomedical perspectives, *Phytochemistry* 67 (17) (2006) 1849–1855, <https://doi.org/10.1016/j.phytochem.2006.06.020>.
- Y. Chen, H. Li, N. Liu, D. Feng, W. Wu, K. Gu, A. Wu, C. Li, X. Wang, Multi-mechanism antitumor/antibacterial effects of Cu-EGCG self-assembling nanocomposite in tumor nanotherapy and drug-resistant bacterial wound infections, *J. Colloid Interface Sci.* 671 (2024) 751–769, <https://doi.org/10.1016/j.jcis.2024.05.080>.
- J. Duan, Z. Chen, X. Liang, Y. Chen, H. Li, K. Liu, L. Gui, X. Wang, Y. Li, J. Yang, Engineering M2-type macrophages with a metal polyphenol network for peripheral artery disease treatment, *Free Radic. Biol. Med.* 213 (2024) 138–149, <https://doi.org/10.1016/j.freeradbiomed.2024.01.014>.
- Q. Li, H. Song, S. Li, P. Hu, C. Zhang, J. Zhang, Z. Feng, D. Kong, W. Wang, P. Huang, Macrophage metabolism reprogramming EGCG-Cu coordination capsules delivered in polyzwitterionic hydrogel for burn wound healing and regeneration, *Bioact. Mater.* 29 (2023) 251–264, <https://doi.org/10.1016/j.bioactmat.2023.07.011>.
- B. Zhang, R. Yao, C. Hu, M.F. Maitz, H. Wu, K. Liu, L. Yang, R. Luo, Y. Wang, Epigallocatechin gallate mediated sandwich-like coating for mimicking endothelium with sustained therapeutic nitric oxide generation and heparin release, *Biomaterials* 269 (2021) 120418, <https://doi.org/10.1016/j.biomaterials.2020.120418>.
- L. Li, Z. Cao, C. Zhang, L. Li, Q. Li, C. Liu, C. Qu, R. Luo, P. Fu, Y. Wang, A versatile passivated protein-adsorption platform for rapid healing of vascular stents by modulating the microenvironment, *Adv. Funct. Mater.* 34 (16) (2024) 2312243, <https://doi.org/10.1002/adfm.202312243>.
- Z. Yang, J. Wang, R. Luo, X. Li, S. Chen, H. Sun, N. Huang, Improved hemocompatibility guided by pulsed plasma tailoring the surface amino functionalities of TiO₂ coating for covalent immobilization of heparin, *Plasma Process Polym.* 8 (9) (2011) 850–858, <https://doi.org/10.1002/ppap.201000101>.
- V.S. Chernonosova, A.A. Gostev, Y. Gao, Y.A. Chesalov, A.V. Shutov, E. A. Pokushalov, A.A. Karpenko, P.P. Laktionov, Mechanical properties and biological behavior of 3D matrices produced by electrospinning from protein-enriched polyurethane, *Biomed Res. Int.* 2018 (2018) 1380606, <https://doi.org/10.1155/2018/1380606>.
- Z. Yang, Q. Tu, M.F. Maitz, S. Zhou, J. Wang, N. Huang, Direct thrombin inhibitor-bivalirudin functionalized allyl plasma polymerized allylamine coating for improved biocompatibility of vascular devices, *Biomaterials* 33 (32) (2012) 7959–7971, <https://doi.org/10.1016/j.biomaterials.2012.07.050>.
- Q. Sun, J. Si, L. Zhao, T. Wei, T. Wang, F. Li, Y. Li, M. Shafiq, L. Wang, R. Liu, D. Zhi, K. Wang, Direct thrombin inhibitor-bivalirudin improved the hemocompatibility of electrospun polycaprolactone vascular grafts, *Compos. B: Eng.* 234 (2022) 109702, <https://doi.org/10.1016/j.compositesb.2022.109702>.
- Q. Wu, T. Xie, Y. Chen, Y. Zhou, X. Han, The effects of bivalirudin and ordinary heparin on the incidence of bleeding events and the level of inflammation after interventional therapy for acute myocardial infarction, *Altern. Ther. Health Med.* (2024).

- [39] P. Du, X. Li, L. Sun, Y. Pan, H. Zhu, Y. Li, Y. Yang, X. Wei, C. Jing, H. Chen, Q. Shi, W. Li, L. Zhao, Improved hemocompatibility by modifying acellular blood vessels with bivalirudin and its biocompatibility evaluation, *J. Biomed. Mater. Res. A* 110 (3) (2022) 635–651, <https://doi.org/10.1002/jbm.a.37316>.
- [40] M. Shafiq, L. Wang, D. Zhi, Q. Zhang, K. Wang, L. Wang, D.H. Kim, D. Kong, S. H. Kim, In situ blood vessel regeneration using neuropeptide substance P-conjugated small-diameter vascular grafts, *J. Biomed. Mater. Res. B Appl. Biomater.* 107 (5) (2019) 1669–1683, <https://doi.org/10.1002/jbm.b.34260>.
- [41] M. Shafiq, S.H. Kim, Covalent immobilization of MSC-affinity peptide on poly(L-lactide-co-ε-caprolactone) copolymer to enhance stem cell adhesion and retention for tissue engineering applications, *Macromol. Res.* 24 (11) (2016) 986–994, <https://doi.org/10.1007/s13233-016-4138-x>.
- [42] J. Zhao, G. Song, Q. Zhao, H. Feng, Y. Wang, J.M. Anderson, H. Zhao, Q. Liu, Development of three-dimensionally printed vascular stents of bioresorbable poly(l-lactide-co-caprolactone), *J. Biomed. Mater. Res. B Appl. Biomater.* 111 (3) (2023) 656–664, <https://doi.org/10.1002/jbm.b.35184>.
- [43] Y. He, W. Liu, L. Guan, J. Chen, L. Duan, Z. Jia, J. Huang, W. Li, J. Liu, X. Xiong, L. Liu, D. Wang, A 3D-printed PLCL scaffold coated with collagen type I and its biocompatibility, *Biomed. Res. Int.* 2018 (2018) 5147156, <https://doi.org/10.1155/2018/5147156>.
- [44] X. Wang, Z. Bai, K. Li, J. Dong, H. Zhang, X. Liu, W. Han, Q. Li, Bioinspired PLCL/Elastin nanofibrous vascular tissue engineering scaffold enhances endothelial cells and inhibits smooth muscle cells, *Biomacromolecules* 24 (6) (2023) 2741–2754, <https://doi.org/10.1021/acs.biomac.3c00175>.
- [45] M.C. Bottino, V. Thomas, G.M. Janowski, A novel spatially designed and functionally graded electrospun membrane for periodontal regeneration, *Acta Biomater.* 7 (1) (2011) 216–224, <https://doi.org/10.1016/j.actbio.2010.08.019>.
- [46] J. Shi, Y. Teng, D. Li, J. He, A.C. Midgley, X. Guo, X. Wang, X. Yang, S. Wang, Y. Feng, Q. Lv, S. Hou, Biomimetic tri-layered small-diameter vascular grafts with decellularized extracellular matrix promoting vascular regeneration and inhibiting thrombosis with the salidroside, *Mater. Today Bio.* 21 (2023) 100709, <https://doi.org/10.1016/j.mtbio.2023.100709>.
- [47] D. Wang, Y. Xu, Q. Li, L.S. Turng, Artificial small-diameter blood vessels: materials, fabrication, surface modification, mechanical properties, and bioactive functionalities, *J. Mater. Chem. B* 8 (9) (2020) 1801–1822, <https://doi.org/10.1039/c9tb01849b>.
- [48] T. Wu, J. Zhang, Y. Wang, B. Sun, M. Yin, G.L. Bowlin, X. Mo, Design and fabrication of a biomimetic vascular scaffold promoting in situ endothelialization and tunica media regeneration, *ACS Appl. Bio. Mater.* 1 (3) (2018) 833–844, <https://doi.org/10.1021/acsabm.8b00269>.
- [49] X. Li, J. Liu, T. Yang, H. Qiu, L. Lu, Q. Tu, K. Xiong, N. Huang, Z. Yang, Mussel-inspired “built-up” surface chemistry for combining nitric oxide catalytic and vascular cell selective properties, *Biomaterials* 241 (2020) 119904, <https://doi.org/10.1016/j.biomaterials.2020.119904>.
- [50] C. Li, F. Wang, P. Ge, Y. Mao, L. Wang, Anti-acute thrombotic surface using coaxial electrospinning coating for vascular graft application, *Mater. Lett.* 205 (2017) 15–19, <https://doi.org/10.1016/j.matlet.2017.06.050>.
- [51] B. Zhang, Y. Qin, L. Yang, Y. Wu, N. Chen, M. Li, Y. Li, H. Wan, D. Fu, R. Luo, L. Yuan, Y. Wang, A polyphenol-network-mediated coating modulates inflammation and vascular healing on vascular stents, *ACS Nano* 16 (4) (2022) 6585–6597, <https://doi.org/10.1021/acsnano.2c00642>.
- [52] Y. Shen, C. Tang, B. Sun, Y. Wu, X. Yu, J. Cui, M. Zhang, M. El-Newehy, H. El-Hamshary, P. Barlis, W. Wang, X. Mo, Development of 3D printed biodegradable, entirely X-ray visible stents for rabbit carotid artery implantation, *Adv. Healthc. Mater.* 13 (15) (2024) 2304293, <https://doi.org/10.1002/adhm.202304293>.
- [53] Y. Shen, Y. Pan, F. Liang, J. Song, X. Yu, J. Cui, G. Cai, M. El-Newehy, M. M. Abdulhameed, H. Gu, B. Sun, M. Yin, X. Mo, Development of 3D printed electrospun vascular graft loaded with tetramethylpyrazine for reducing thrombosis and restraining aneurysmal dilatation, *Burns & Trauma* 12 (2024) tkae008, <https://doi.org/10.1093/burnst/tkae008>.
- [54] D. Tang, S. Chen, D. Hou, J. Gao, L. Jiang, J. Shi, Q. Liang, D. Kong, S. Wang, Regulation of macrophage polarization and promotion of endothelialization by NO generating and PEG-YIGSR modified vascular graft, *Mater. Sci. Eng. C Mater. Biol. Appl.* 84 (2018) 1–11, <https://doi.org/10.1016/j.msec.2017.11.005>.
- [55] Z. Wang, Y. Lu, K. Qin, Y. Wu, Y. Tian, J. Wang, J. Zhang, J. Hou, Y. Cui, K. Wang, J. Shen, Q. Xu, D. Kong, Q. Zhao, Enzyme-functionalized vascular grafts catalyze in-situ release of nitric oxide from exogenous NO prodrug, *J. Control. Release.* 210 (2015) 179–188, <https://doi.org/10.1016/j.jconrel.2015.05.283>.
- [56] M.A.A. Fahad, H.-Y. Lee, S. Park, M. Choi, P.C. Shanto, M. Park, S.H. Bae, B.-T. Lee, Small-diameter vascular graft composing of core-shell structured micro-nanofibers loaded with heparin and VEGF for endothelialization and prevention of neointimal hyperplasia, *Biomaterials* 306 (2024) 122507, <https://doi.org/10.1016/j.biomaterials.2024.122507>.
- [57] Y. Chen, Z. Yuan, W. Sun, M. Shafiq, J. Zhu, J. Chen, H. Tang, L. Hu, W. Lin, Y. Zeng, L. Wang, L. Zhang, Y. She, H. Zheng, G. Zhao, D. Xie, X. Mo, C. Chen, Vascular endothelial growth factor-recruiting nanofiber bandages promote multifunctional skin regeneration via improved angiogenesis and immunomodulation, *Adv. Mater.* 5 (1) (2023) 327–348, <https://doi.org/10.1007/s42765-022-00226-8>.
- [58] B. Yi, Y. Shen, H. Tang, X. Wang, B. Li, Y. Zhang, Stiffness of aligned fibers regulates the phenotypic expression of vascular smooth muscle cells, *ACS Appl. Mater. Interfaces* 11 (7) (2019) 6867–6880, <https://doi.org/10.1021/acsami.9b00293>.
- [59] T.H. Pham, N.M. Trang, E.N. Kim, H.G. Jeong, G.S. Jeong, Citriopten inhibits vascular smooth muscle cell proliferation and migration via the TRPV1 receptor, *ACS Omega* 9 (27) (2024) 29829–29839, <https://doi.org/10.1021/acsomega.4c03539>.
- [60] A. Gharimti, Z.A. Kanafani, Vascular graft infections: an update, *Infect. Dis. Clin. North Am.* 32 (4) (2018) 789–809, <https://doi.org/10.1016/j.idc.2018.06.003>.
- [61] D. Zhang, Q. Chen, C. Shi, M. Chen, K. Ma, J. Wan, R. Liu, Dealing with the foreign-body response to implanted biomaterials: strategies and applications of new materials, *Adv. Funct. Mater.* 31 (6) (2021) 2007226, <https://doi.org/10.1002/adfm.202007226>.
- [62] L. Li, C. Chen, C. Zhang, R. Luo, X. Lan, F. Guo, L. Ma, P. Fu, Y. Wang, A honokiol-mediated robust coating for blood-contacting devices with anti-inflammatory, antibacterial and antithrombotic properties, *J. Mater. Chem. B* 9 (47) (2021) 9770–9783, <https://doi.org/10.1039/d1tb01617b>.
- [63] A.S. Klar, K. Michalak-Micka, T. Biedermann, C. Simmen-Meuli, E. Reichmann, M. Meuli, Characterization of M1 and M2 polarization of macrophages in vascularized human dermo-epidermal skin substitutes in vivo, *Pediatr. Surg. Int.* 34 (2) (2018) 129–135, <https://doi.org/10.1007/s00383-017-4179-z>.
- [64] M. Rafique, T. Wei, Q. Sun, A.C. Midgley, Z. Huang, T. Wang, M. Shafiq, D. Zhi, J. Si, H. Yan, D. Kong, K. Wang, The effect of hypoxia-mimicking responses on improving the regeneration of artificial vascular grafts, *Biomaterials* 271 (2021) 120746, <https://doi.org/10.1016/j.biomaterials.2021.120746>.
- [65] J. Zhang, Q. Cui, Y. Zhao, R. Guo, C. Zhan, P. Jiang, P. Luan, P. Zhang, F. Wang, L. Yang, X. Yang, Y. Xu, Mechanism of angiogenesis promotion with Shexiang Baixin Pills by regulating function and signaling pathway of endothelial cells through macrophages, *Atherosclerosis* 292 (2020) 99–111, <https://doi.org/10.1016/j.atherosclerosis.2019.11.005>.
- [66] Y. Xiao, X. Jin, L. Jia, J. Li, B. Zhang, X. Geng, L. Ye, A.-Y. Zhang, Y. Gu, Z.-G. Feng, Long-term observation of polycaprolactone small-diameter vascular grafts with thickened outer layer and heparinized inner layer in rabbit carotid arteries, *Biomed. Mater.* 19 (3) (2024) 035018, <https://doi.org/10.1088/1748-605X/ad2f6b>.
- [67] Q. Cai, W. Liao, F. Xue, X. Wang, W. Zhou, Y. Li, W. Zeng, Selection of different endothelialization modes and different seed cells for tissue-engineered vascular graft, *Bioact. Mater.* 6 (8) (2021) 2557–2568, <https://doi.org/10.1016/j.bioactmat.2020.12.021>.
- [68] M. Rodríguez, J.A. Kluge, D. Smoot, M.A. Kluge, D.F. Schmidt, C.R. Paetsch, P. S. Kim, D.L. Kaplan, Fabricating mechanically improved silk-based vascular grafts by solution control of the gel-spinning process, *Biomaterials* 230 (2020) 119567, <https://doi.org/10.1016/j.biomaterials.2019.119567>.
- [69] M. Generali, E.A. Casanova, D. Kehl, D. Wanner, S.P. Hoerstrup, P. Cinielli, B. Weber, Autologous endothelialized small-caliber vascular grafts engineered from blood-derived induced pluripotent stem cells, *Acta Biomater.* 97 (2019) 333–343, <https://doi.org/10.1016/j.actbio.2019.07.032>.
- [70] Y. Yang, D. Lei, H. Zou, S. Huang, Q. Yang, S. Li, F.-L. Qing, X. Ye, Z. You, Q. Zhao, Hybrid electrospun rapamycin-loaded small-diameter decellularized vascular grafts effectively inhibit intimal hyperplasia, *Acta Biomaterialia* 97 (2019) 321–332, <https://doi.org/10.1016/j.actbio.2019.06.037>.
- [71] P. Karuppuswamy, J. Reddy Venugopal, B. Navaneethan, A. Luwang Laiva, S. Ramakrishna, Polycaprolactone nanofibers for the controlled release of tetracycline hydrochloride, *Mater. Lett.* 141 (2015) 180–186, <https://doi.org/10.1016/j.matlet.2014.11.044>.
- [72] M. Zhu, Y. Wu, W. Li, X. Dong, H. Chang, K. Wang, P. Wu, J. Zhang, G. Fan, L. Wang, J. Liu, H. Wang, D. Kong, Biodegradable and elastomeric vascular grafts enable vascular remodeling, *Biomaterials* 183 (2018) 306–318, <https://doi.org/10.1016/j.biomaterials.2018.08.063>.
- [73] Z. Yuan, M. Shafiq, H. Zheng, L. Zhang, Z. Wang, X. Yu, J. Song, B. Sun, M. El-Newehy, H. El-Hamshary, Y. Morsi, C. Wang, X. Mo, Y. Xu, Multi-functional fibrous dressings for infectious injury treatment with anti-adhesion wound healing, *Mater. Design* 235 (2023) 112459, <https://doi.org/10.1016/j.matdes.2023.112459>.
- [74] A. Das, A. Nikhil, A. Kumar, Antioxidant and trilayered electrospun small-diameter vascular grafts maintain patency and promote endothelialization in rat femoral artery, *ACS Biomater. Sci. Eng.* 10 (3) (2024) 1697–1711, <https://doi.org/10.1021/acsbomaterials.4c00006>.
- [75] T. Wu, J. Zhang, Y. Wang, D. Li, B. Sun, H. El-Hamshary, M. Yin, X. Mo, Fabrication and preliminary study of a biomimetic tri-layer tubular graft based on fibers and fiber yarns for vascular tissue engineering, *Mater. Sci. Eng. C Mater. Biol. Appl.* 82 (2018) 121–129, <https://doi.org/10.1016/j.msec.2017.08.072>.
- [76] P. Liu, X. Liu, L. Yang, Y. Qian, Q. Lu, A. Shi, S. Wei, X. Zhang, Y. Lv, J. Xiang, Enhanced hemocompatibility and rapid magnetic anastomosis of electrospun small-diameter artificial vascular grafts, *Front. Bioeng. Biotechnol.* 12 (2024), <https://doi.org/10.3389/fbioe.2024.1331078>.
- [77] F. Zhang, L. Yang, C. Hu, L. Li, J. Wang, R. Luo, Y. Wang, Phosphorylcholine- and cation-bearing copolymer coating with superior antibiofilm and antithrombotic properties for blood-contacting devices, *J. Mater. Chem. B* 8 (36) (2020) 8433–8443, <https://doi.org/10.1039/d0tb01662d>.
- [78] R. Deana, L. Turetta, A. Donella-Deana, M. Donà, A.M. Brunati, L. De Michiel, S. Garbisa, Green tea epigallocatechin-3-gallate inhibits platelet signalling pathways triggered by both proteolytic and non-proteolytic agonists, *Thrombos. Haemostas.* 89 (5) (2003) 866–874.
- [79] B. Zhang, Y. Qin, Y. Wang, A nitric oxide-eluting and REDV peptide-conjugated coating promotes vascular healing, *Biomaterials* 284 (2022) 121478, <https://doi.org/10.1016/j.biomaterials.2022.121478>.
- [80] A. de Mel, F. Murad, A.M. Seifalian, Nitric oxide: a guardian for vascular grafts? *Chem. Rev.* 111 (9) (2011) 5742–5767, <https://doi.org/10.1021/cr200008n>.
- [81] Y. Hu, L. Li, Q. Li, S. Pan, G. Feng, X. Lan, J. Jiao, L. Zhong, L. Sun, A biomimetic tri-phasic scaffold with spatiotemporal patterns of gastrin to regulate

- hierarchical tissue-based vascular regeneration, *Bioact. Mater.* 38 (2024) 512–527, <https://doi.org/10.1016/j.bioactmat.2024.05.007>.
- [82] S.K. Nicholson, G.A. Tucker, J.M. Brameld, Effects of dietary polyphenols on gene expression in human vascular endothelial cells, *Proc. Nutr. Soc.* 67 (1) (2008) 42–47, <https://doi.org/10.1017/S0029665108006009>.
- [83] M. Clément, J. Chappell, J. Raffort, F. Lareyre, M. Vandestienne, A.L. Taylor, A. Finigan, J. Harrison, M.R. Bennett, P. Bruneval, S. Taleb, H.F. Jørgensen, Z. Mallat, Vascular smooth muscle cell plasticity and autophagy in dissecting aortic aneurysms, *Arterioscleros., Thrombos. Vascul. Biol.* 39 (6) (2019) 1149–1159, <https://doi.org/10.1161/ATVBAHA.118.311727>.
- [84] J. Shi, X. Zhang, L. Jiang, L. Zhang, Y. Dong, A.C. Midgley, D. Kong, S. Wang, Regulation of the inflammatory response by vascular grafts modified with Aspirin-Triggered Resolvin D1 promotes blood vessel regeneration, *Acta Biomater.* 97 (2019) 360–373, <https://doi.org/10.1016/j.actbio.2019.07.037>.
- [85] W. Ma, Z. Liu, T. Zhu, L. Wang, J. Du, K. Wang, C. Xu, Fabric-enhanced vascular graft with hierarchical structure for promoting the regeneration of vascular tissue, *Adv. Healthc. Mater.* (2024) e2302676.
- [86] X. Hou, S. Yang, J. Yin, Blocking the REDD1/TXNIP axis ameliorates LPS-induced vascular endothelial cell injury through repressing oxidative stress and apoptosis, *Am. J. Physiol. Cell Physiol.* 316 (1) (2019) C104–C110, <https://doi.org/10.1152/ajpcell.00313.2018>.
- [87] J. He, S. Zhou, J. Wang, B. Sun, D. Ni, J. Wu, X. Peng, Anti-inflammatory and anti-oxidative electrospun nanofiber membrane promotes diabetic wound healing via macrophage modulation, *J. Nanobiotechnology* 22 (1) (2024) 116, <https://doi.org/10.1186/s12951-024-02385-9>.
- [88] R. Johnson, M. Rafuse, P.P. Selvakumar, W. Tan, Effects of recipient age, heparin release and allogeneic bone marrow-derived stromal cells on vascular graft remodeling, *Acta Biomaterialia* 125 (2021) 172–182, <https://doi.org/10.1016/j.actbio.2021.02.028>.